LLNL-JRNL-692614

Plutonium Partitioning in Glassy Aerodynamic Fallout from a Nuclear Weapon Test

K. S. Holliday, J. M. Dierken, M. L. Monroe, M. A. Fitzgerald, N. E. Marks, R. C. Gostic, K. B. Knight, I. D. Hutcheon, J. W. McClory

May 24, 2016

Dalton Transactions

LLNL-JRNL-69261

Plutonium Segregation in Glassy Aerodynamic Fallout from a Nuclear Weapon Test

K. S. Holliday,[a*] J. M. Dierken,[b] M. L. Monroe,[b] M. A. Fitzgerald,[a,c] N. E. Marks,[a] R. C. Gostic,[a] K. B. Knight,[a] K. R Czerwinski,[c] I. D. Hutcheon[a] and J. W. McClory[b]

This study combines electron microscopy equipped with energy dispersive spectroscopy to probe major element composition and autoradiography to map plutonium in order to examine the spatial relationships between plutonium and fallout composition in aerodynamic glassy fallout from a nuclear weapon test. A sample set of 48 individual fallout specimens were interrogated to reveal that the significant chemical heterogeneity of this sample set could be described compositionally with a relatively small number of compositional endmembers. Furthermore, high concentrations of plutonium were never associated with several endmember compositions and concentrated with the so-called mafic glass endmember. This result suggests that it is the physical characteristics of the compositional endmembers and not the chemical characteristics of the individual component elements that govern the un-burnt plutonium distribution with respect to major element composition in fallout.

Introduction

The blast, thermal, and radiation effects of nuclear weapons have been well studied and documented.[1,2] More than 200 source documents were compiled into a succinct report describing fallout particles in 1965.[3] This report highlights the early subjects of study: fractionation of debris, deposition of radioactivity from the fallout plume, and radioactive materials leaching into the environment. Fractionation is defined as “any alteration of radionuclide composition occurring between the time of detonation and the time of radiochemical analysis which causes the debris sample to be non-representative of the detonation products taken as a whole”.[4] This is an important factor for determining how the various fission products and unburnt fuel vary with respect to each other[5,6]; however, this phenomena does little to explain where radioactive material concentrate in fallout other than refractory materials tend to concentrate closer to ground zero[7], while volatile species are depleted in this area.[8] Studies that determined where activity was distributed were focused on total activity, which at the time was dominated by fission products.[9] The radionuclides of greatest concern during the nuclear weapons testing era were tritium[10] and relatively long lived fission products such as Sr-90.[11]

This year marks 20 years since the introduction of the Comprehensive Test Ban Treaty, and while it has yet to enter into force, it represents a significant reduction in nuclear tests worldwide. Today, residual actinides are the species of greatest concern in the post-test era. In

[a]Lawrence Livermore National Laboratory, 7000 East Avenue Livermore CA USA 94550
[b]Air Force Institute of Technology, Wright-Patterson AFB Dayton OH USA 45433
[c]University of Nevada Las Vegas, 4505 Maryland Parkway Las Vegas NV USA 89154
*corresponding author
Additional information available in electronic supplementary information (ESI)

particular, the mobility of plutonium is a significant environmental uncertainty.[12-14] Nuclear weapon testing is the dominant source of transuranic elements in the environment.[11] While the initial radioactivity following a nuclear weapon test is dominated by fission products, the long term radioactivity, and therefore the long term environmental impact, is predominantly due to actinides. For example, at the Nevada National Security Site (formerly Nevada Test Site), there is an estimated 4 x 10^{16} Bq of radioactivity from actinide elements, most of which is a result of plutonium.[12] Similar trends in activity distributions are seen at other sites around the world, such as Reggane in Algeria,[13] and Semipalatinsk in Kazakhstan.[14] Even if one considers only near-surface bursts that resulted in vitrified sand/soil, the estimated number of tests conducted still approaches 100, distributed in approximately 10 different sites.[15] Today, the most significant environmental impact of the testing era is the remaining actinides, in particular plutonium, and its mobility.[12-15]

The bulk chemical composition of glassy fallout mimics the compositional character of the local soil.[16] This is due in large part to the limited thermal diffusivity of the soil and the short timescales involved. The thermal radiation is limited in its penetration depth so that only 8.5% of the available thermal energy is used in the heating of the surrounding material.[17] A large portion of the glassy fallout material is generated from soil being sucked into the vacuum created by the hot cloud rise, where it is subsequently melted and then redeposited as local fallout.[18-20] If the material cools enough to solidify while in the air, it produces aerodynamic fallout particles as described by Adams *et al*.[21] These aerodynamic fallout objects show higher amounts of unburnt fuel and fission products as compared to other glassy material typically referred to as trinitite, puddle glass, or ground glass.[18,22-24] In this scenario of aerodynamic fallout formation, soil is swept into the hot cloud, melted, and then solidified before returning to the surface. This leaves a relatively short time for homogenizing the soil components in the molten state, resulting in significant compositional heterogeneity in these fallout particles.[25] The timeframe for this scenario is estimated to be approximately 2 seconds in some tests.[26] A study using microanalytical techniques reported $^{235}U/^{238}U$ ratios within small areas varying over three orders of magnitude.[25] This same study found that in some cases the unburnt fuel component seemed to correlate with major element composition.

In order to understand how actinides behave in fallout materials, a number of studies have investigated spatial correlation and microscale characterization of fallout from the first nuclear test, Trinity.[18,19,27-30] This test was an approximately 20 kt implosion device that was detonated on top of a 30 m tall steel tower. The tower was used to mimic an air burst, the eventual destiny of “fat man”, the bomb for which the test was conducted. Work on aerodynamic glassy fallout as well as on “trinitite” (also referred to as “ground glass” or “puddle glass”) has revealed a correlation between Pb and Cu that is attributed to anthropogenic sources.[27,28] Others have reported correlations between the concentrations of certain major elements and the distribution of U, Pu, and ^{137}Cs in fallout.[21,29] These works revealed an anti-correlation between these radionuclides and the minerals quartz and K-feldspar that are present in the trinitite as crystalline inclusions. In contrast, a positive correlation appears to exist between these radionuclides and Fe and Ca. The correlation with Fe is somewhat expected in the case of Trinity because of the large quantity of steel used for the tower, but the correlation of Pu and Ca remains unexplained. The bulk of these studies have investigated trinitite, and little attention has been given to aerodynamic glassy fallout, which contains more unburnt plutonium relative to other glassy fallout (i.e. trinitite, puddle glass, ground glass).

In this study we have combined spatially resolved elemental concentration measurements and autoradiographic images of actinide activity in order to characterize the distribution of Pu relative to major element composition in aerodynamic fallout. The samples selected are derived from a Pu-fueled test other than Trinity, and therefore provide an excellent opportunity to understand plutonium distribution and associations. The test sampled was a near-surface burst, which did not have an associated steel tower. We have selected aerodynamic glassy fallout because of the higher amount of plutonium within the sample. Additionally, by sampling a nuclear test that did not have the massive steel tower that contributed to the Trinity fallout, we hope to minimize the impact of anthroprogenic Fe. In this study we demonstrate that Pu is preferentially associated with specific glass compositions. We further propose possible drivers for this behavior that could be tested either in the laboratory or by analyzing historical nuclear test fallout.

Experimental

Samples were collected near ground zero of a plutonium fueled, near-surface detonation along the direction that the fallout plume traveled. Soil within 10 cm of the surface in this area was then sieved to collect ~1 mm-diameter particles. Glassy spheroid particles were selected by inspection with an optical microscope (Leica M165), yielding samples consisting of aerodynamically cooled glassy fallout, and a random subset was selected for the present study. A total of 48 samples were selected for this study. All data presented are from samples collected from the same location, and selected from the same size fraction. The samples were mounted in a pre-drilled aluminum puck with epoxy to aid in polishing. The samples were then polished to a mirror finish exposing the approximate mid-plane of each fallout object.

The alpha and beta particle detection was performed using a Ludlum Model 3030 Alpha-Beta Sample Counter in order to get an estimate of relative activities. The autoradiography was accomplished with a film changing tent, super resolution imaging plate, which was developed in a FUJIFILM FLA-7000 fluorescent image analyzing system. All samples were exposed at the same time over approximately 24 hours. The resulting maps of activity are dominated by the plutonium within the sample because of both the specific activity of Pu and the short range of the alpha particles that are emitted. In contrast, beta particles produce more diffuse maps, which lack the resolution required to distinguish features in these samples.[31]

Electron microscopy was performed on a FEI Inspect F scanning electron microscope. After polishing to a mirror finish, samples were prepared by sputtering a 100 angstrom coating of carbon to prevent charging. Micrographs were collected in both secondary electron and backscattered electron mode using an accelerating voltage of 15 kV, working distance of 11.5 mm, and a spot size of 5.5. Energy dispersive spectroscopy mapping was performed using an EDAX silicon drift detector. In the course of analyzing the sample suite of aerodynamic glassy fallout samples, it was recognized that the major element composition could be described by a small number of endmember compositions or mixtures thereof. Here we use the term endmember as discrete compositional regions that exist within the sample set, and those regions can be combined to describe compositional variations due to mixing. These may or may not correspond to geological endmember minerals within the soil. EDS point analyses were performed to measure each unique area of composition present within the sample. As such, the number of analyses is only loosely related to abundance. For instance, a homogeneous sample was analyzed with only 3-5 points to confirm homogeneity; whereas, the most heterogeneous sample that had a large degree of mixing was analyzed with 38 points to adequately describe the composition. The complete data set can be found in supplemental information.

All images (SEM, autoradiography, and EDS maps) were contrast-adjusted to emphasize the heterogeneity within each sample. No effort was made to apply consistent brightness and gain settings one sample to the next. All single element maps of a sample were adjusted together so that the relative amounts of each element within a sample could be evaluated. Image processing, including estimates of modal abundance, were performed with ImageJ image processing and analysis software using the thresholding features.[32] Thermodynamic calculations for various glass compositions were accomplished with the thermodynamic modeling software rhyolite-MELTS in order to determine viscocities.[33]

Results and Discussion

Major Element Composition

The relative abundance of each endmember is discussed in a later section. In all, 546 individual spot analyses of major element composition were measured over the sample set (see supplemental information for complete data set). Four endmember compositions were identified: (1) mafic glass, (2) SiO_2-dominant, (3) felsic glass, or (4) apparent inclusions (small areas with high concentrations of Ca, Zr, Mg, or Fe as oxide). Each of these compositions is described in detail below.

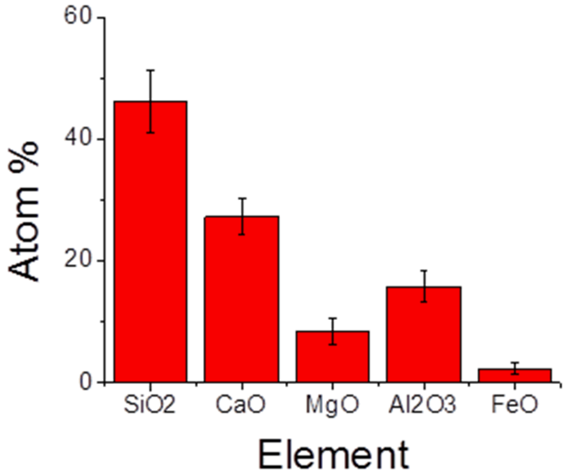

Figure 1: Elemental composition of mafic glass endmember ($Si_{0.46}Ca_{0.28}Al_{0.16}Mg_{0.08}Fe_{0.02}O_{1.55}$). Elements assumed to be present as oxides within the glass. Error bars represent standard deviation (1 sigma) across the sample suite.

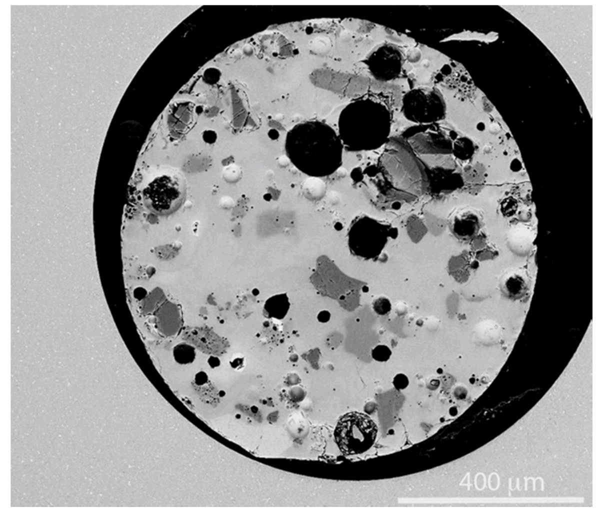

Figure 2: Backscattered electron image of spherical glassy fallout. Medium-gray area making up the majority of the sphere can be characterized as the mafic glass endmember composition.

(1) The mafic glass composition makes up the majority of each sphere and is the most abundant composition found for this sample set. The average composition of this endmember and the standard deviation within the measurements is presented in Figure 1. An example of the mafic glass endmember can be seen in the backscattered electron image of Figure 2, where it appears as the medium gray area making up the majority of the sphere. Because glasses are non-stoichiometric, it is convenient to write their composition with the cations summing to one and the corresponding oxygen stoichiometry calculated. For the average mafic glass endmember composition this is written as: $Si_{0.46}Ca_{0.28}Al_{0.16}Mg_{0.08}Fe_{0.02}O_{1.55}$. The mafic glass composition is the dominant source of calcium, magnesium, and iron in this sample set.

(2) The SiO_2-dominant endmember composition is nearly pure SiO_2, presumably originating from quartz in the soil. Because of its lower average Z, this end-member appears darker in the backscattered electron images as can be seen in Figure 3. The SiO_2 compositional endmember can be described as both a relatively well defined region which does not exhibit significant mixing with other phases (Figure 3a) or as a diluent of the mafic glass composition, when significant mixing is evident (Figure 3b).

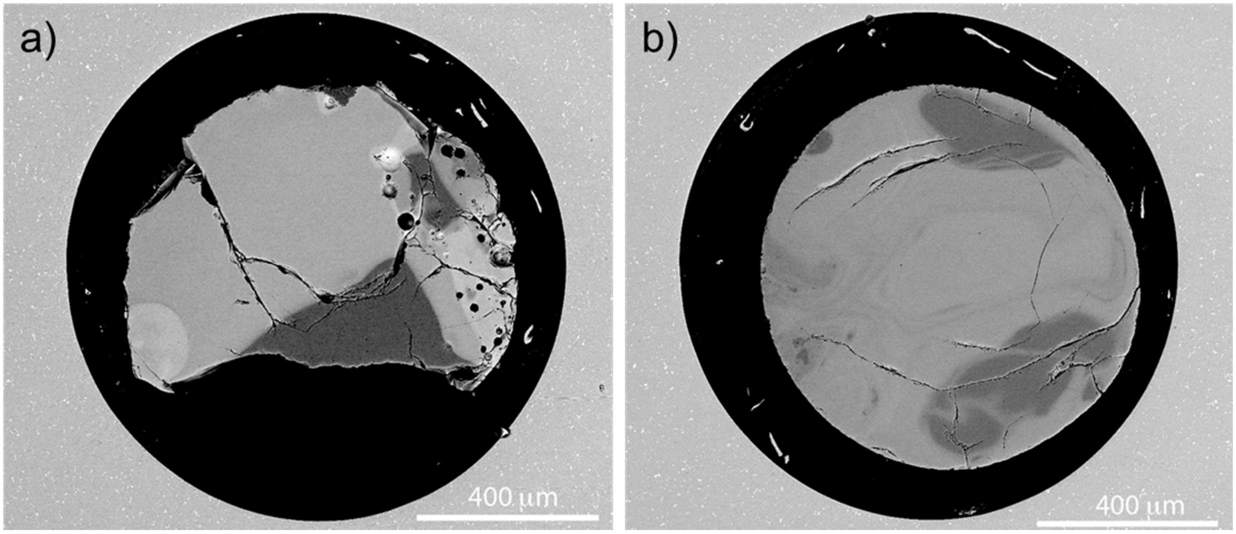

Figure 3: Examples of SiO_2 endmember composition (dark gray) in fallout. a) Angular SiO_2 region with little evidence of mixing and b) SiO_2 regions that show evidence of mixing both by diffusion and convection.

(3) The felsic glass endmember composition can be written as $Si_{0.63}Al_{0.20}K_{0.12}Na_{0.04}O_{1.64}$ and is the dominant source of sodium and potassium within these samples. The average composition of this endmember and the standard deviation in the measurements is presented in Figure 4. The zones of felsic glass composition are often porous as can be seen in Figure 5. It should be noted that both the felsic glass and mafic glass endmember compositions contain aluminum at similar concentrations.

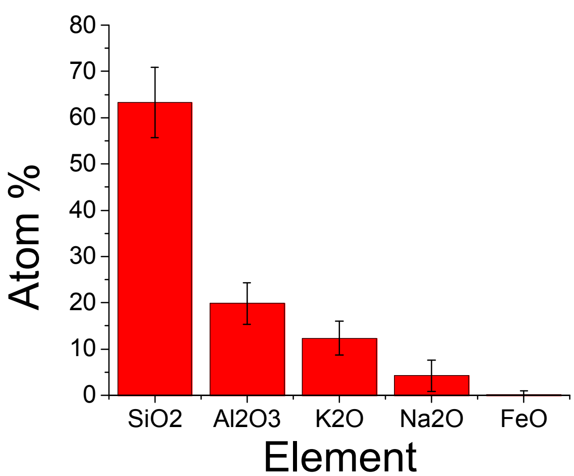

Figure 4: Elemental composition of the feldsic glass endmember ($Si_{0.63}Al_{0.20}K_{0.12}Na_{0.04}O_{1.64}$). Elements assumed to be present as oxides within the glass. Error bars represent standard deviation (1 sigma).

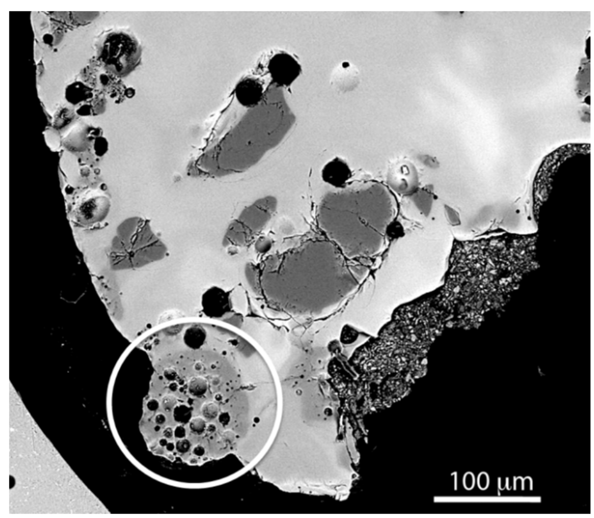

Figure 5: Backscattered electron image of a region of spherical glassy fallout. Porous surface inclusion at bottom left (circled) can be characterized as the felsic glass endmember composition.

(4) Uncommonly, a small region was enriched in a single element above those concentrations previously described in endmember compositions. These were characterized as "apparent inclusions" and represent the lowest modal abundance in these samples. The elements that were found as apparent inclusions were Ca (6 samples), Mg (5 samples), Zr (4 samples), and Fe (2 samples). Calcium as calcite, zirconium as zircon, and magnesium in a range of minerals are common minor components of soil. Iron has both natural and anthropogenic source possibilities and was only evident in two samples. Both examples of high iron were associated with measurable amounts of titanium and one was associated with manganese. With only this information it is impossible to clearly identify a source term for iron. An example of each of these types of regions is found in Figure 6 a-d.

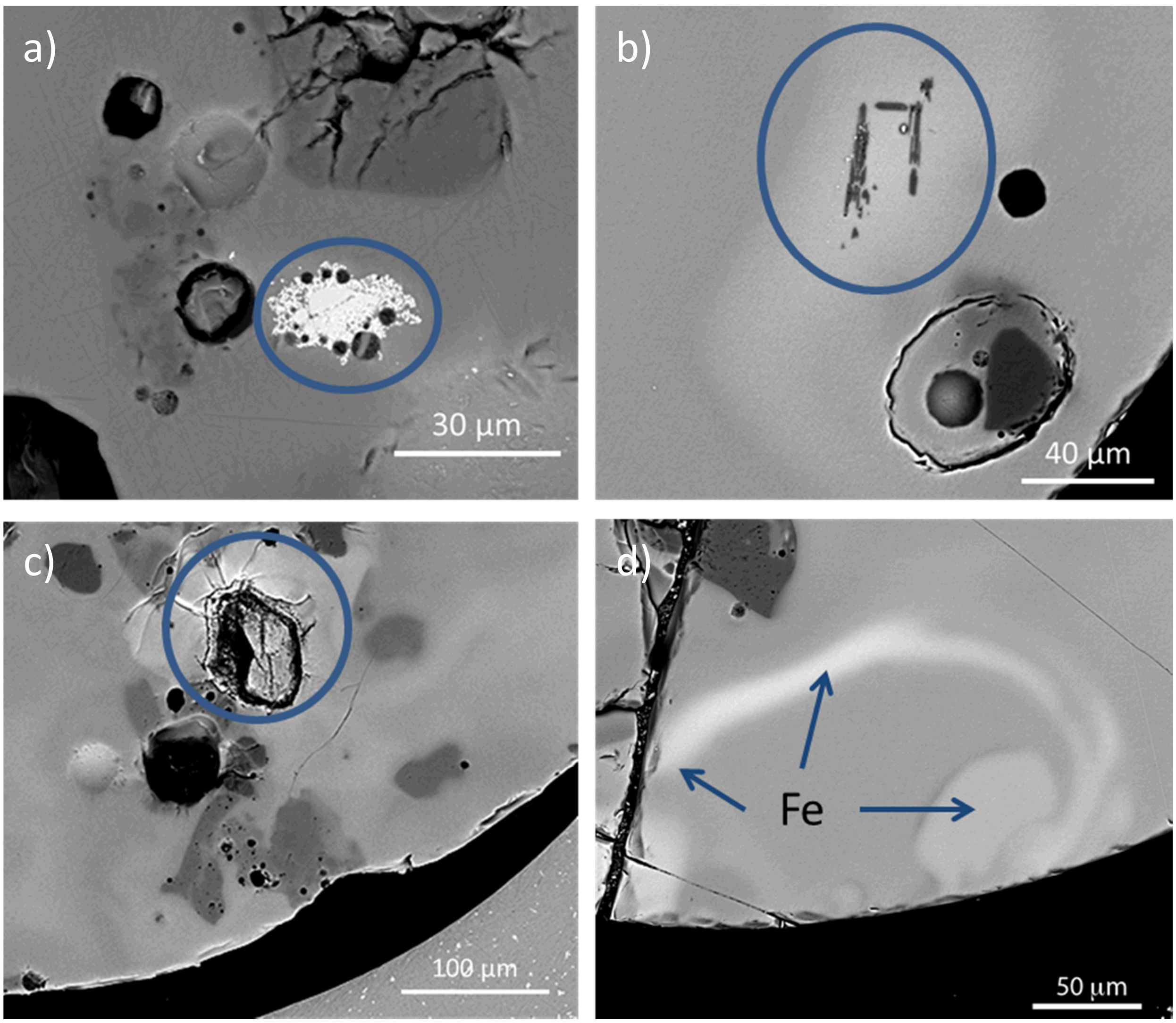

Figure 6: An example of each element found in high concentrations within a small area. a) zirconium b) magnesium c) calcium and d) iron.

Endmember Abundances

Using the gray-scale backscattered electron micrographs it is possible to quantify the modal abundance of each endmember domain and vesicles by setting thresholds that highlight those features which have the same backscatter intensity. For glassy fallout samples this can be difficult. These materials tend not to have significant contrast in mean atomic number. Also, the amount of diffusion and mixing leads to gradational boundaries that are subject to definition by the user. With these limitations in mind, it is still possible to get a sense of the relative quantity of vesicles and each endmember composition within the sample set.

It was found that 35% (17 out of 48) of these fallout samples appeared largely homogeneous by SEM backscattered imaging such as Figure 7. Vesicles made up 10% of all samples, but varied from zero vesicles (Fig. 7) to 54% of the cross sectioned area (Fig. 8). The modal abundance of the endmember glass compositions that makes up these samples (which is to say excluding pore space and homogeneous samples) is 86% mafic glass, 9.4% SiO_2, 4.5% felsic glass, and 0.6% other inclusions such as Ca, Fe, Zr, or Mg oxides. See table 1 for a summary of modal abundances.

Table 1: Number of samples and modal abundances as determined by thresholding backscattered electron images. Data for endmember abundances are given excluding homogeneous samples, which are a mixture of these endmembers. They are also reported without including the area occupied by vesicles.

	# of samples (>50% area)	% of all sample area	% of heterogeneous samples	% of heterogeneous samples excluding voids
Homogeneous	17	35.4		
Heterogeneous	31	54.1		
Void space		10.5	16.9	
Mafic glass			71.9	85.5
SiO2			7.9	9.4
Felsic glass			3.8	4.5
Other inclusions			0.5	0.6

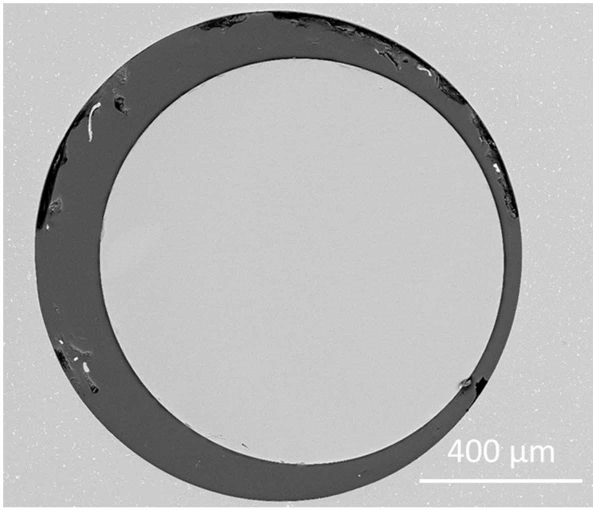

Figure 7: An example of homogeneous glassy fallout by backscattered electron microscopy.

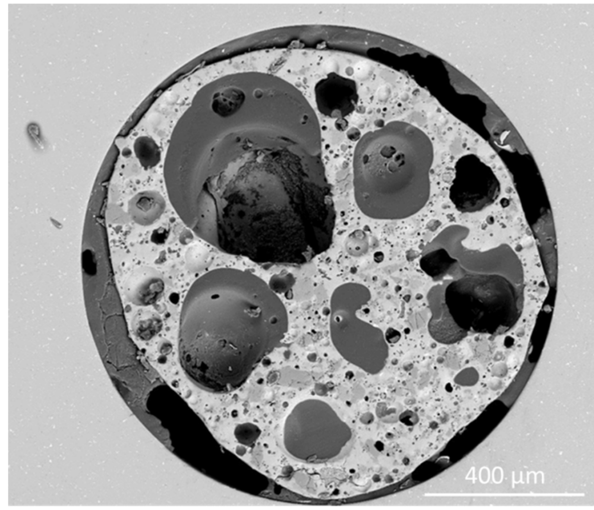

Figure 8: An example of highly vesicular glassy fallout by backscattered electron microscopy.

Correlating Pu to Major Element Composition

It has been shown that condensation mechanisms are not the driving force for major element composition in fallout of this size fraction.[34] Instead a simple melting and mixing model adequately describes the major element variations found in these samples. Based on image analysis and EDS, we have identified endmember compositions that are the source of major element compositions. By analyzing endmember mixing relationships and Pu distribution, it is possible to identify trends in plutonium segregation within this sample set.

The autoradiography maps were compared to major element composition with an interest not in individual element correlations, but with respect to endmember compositions. Although four endmember compositions were identified, only mafic glass was associated with elevated plutonium activity. Felsic glass, pure SiO_2, and small areas with elevated concentrations of a single element were never associated with high levels of activity. The complete set of backscattered electron images and autoradiography can be found in supplemental information. An example can be seen in the large SiO_2 region, which corresponds to a significant drop in activity in Figure 9.

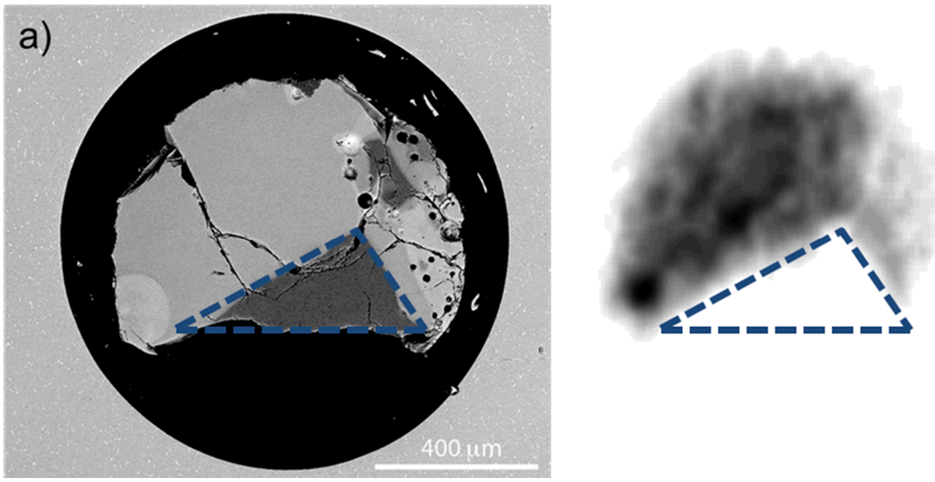

Figure 9: Backscattered electron image (left) showing that a large angular SiO_2 region (dark gray) corresponds to an absence of activity in the autoradiograph (outlined region in the right-hand image). Darker areas of autoradiograph (right) are a result of increased radioactivity due to higher Pu concentration.

This positive correlation between activity and the mafic glass endmember can also be visualized when the mafic glass is diluted by felsic or SiO_2 melt. It was previously shown that the mafic glass composition is the predominant source of calcium, magnesium, and iron. It is therefore possible to show the localization of the mafic glass end-member as the map of any of these elements (in the absence of other sources such as CaO or FeO inclusions). Figure 10 shows an example where the plutonium concentration clearly follows the mafic glass end-member, which is approximated by the calcium SEM/EDS map.

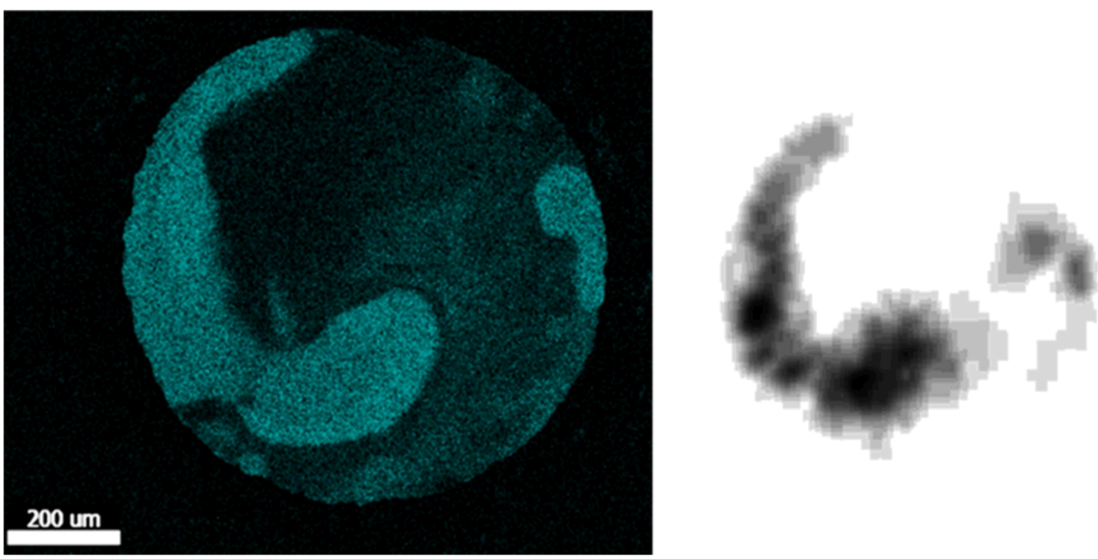

Figure 10: SEM/EDS map of calcium concentration (left, lighter area is higher Ca) as an indication of mafic glass endmember concentration compared to an autoradiograph (right). Darker areas of autoradiograph (right) are a result of increased radioactivity due to higher Pu concentration.

It is important to note that this is a relationship between plutonium and the mafic glass endmember composition, not specifically calcium. This difference becomes evident when comparing autoradiographs and small regions of enriched calcium (in excess of the calcium content of mafic glass composition) as seen in Figure 11. Although activity is correlated with calcium, magnesium, and iron associated with the mafic glass composition, it is never associated with inclusion-like areas enriched in a single element even if that element is calcium, magnesium, or iron (Figure 11). This observation suggests that plutonium segregation in these samples is associated with the mafic glass endmember composition and not specifically with Ca or Fe. Accordingly, this suggests that the physical properties of the compositional endmembers, rather than the chemistry of a single element, are what dictates the relative distribution of plutonium in this suite of fallout samples. Wallace et al.[29] hypothesized that the correlations were due to melting point temperature of the various compositions. The melting point of our endmembers suggests that this may not be the case. While the melting point of SiO_2 (1600°C) is higher than the mafic glass (1261°C) that incorporates plutonium, the felsic glass composition has a lower melting point (720°C) still and is anti-correlated with plutonium. It is possible that viscosity is a driving factor for plutonium incorporation, since the mafic glass composition has lower viscosity than both the felsic glass endmember and SiO_2. A plot of viscosity vs. temperature, calculated using rhyolite-MELTS, can be found in Figure 12. Viscosity seems to be one of the only physical properties in which mafic glass composition is not bracketed by pure SiO_2 and felsic glass. It is possible that the lower viscosity of the mafic glass leads to a greater degree of mixing and therefore plutonium incorporation into the bulk. Further investigation with a wider array of samples is required to determine if viscosity is a dominant characteristic for plutonium incorporation into fallout.

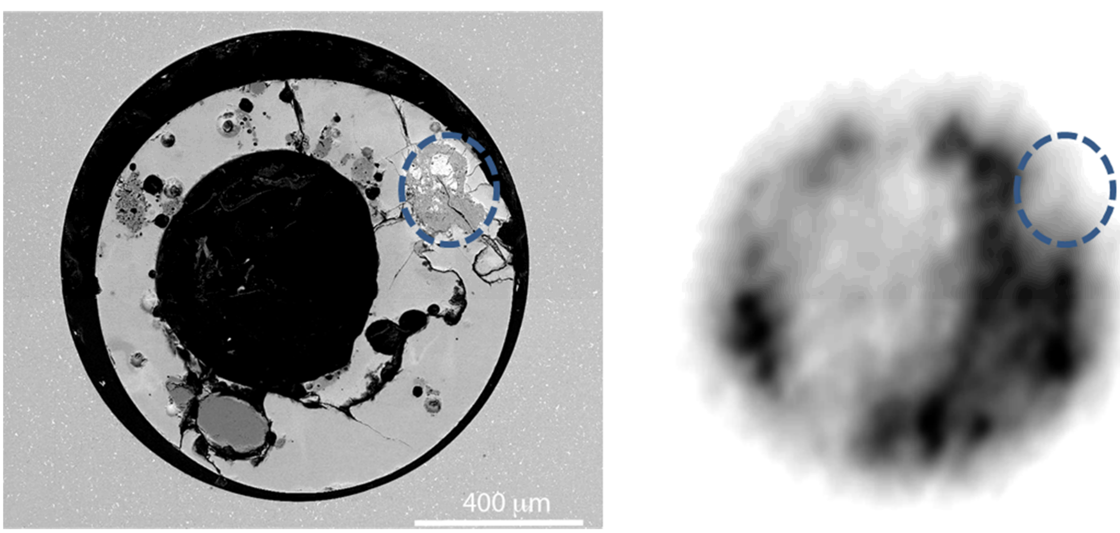

Figure 11: Backscattered electron image (left) showing a large calcium-rich inclusion (circled) which corresponds to a drop in activity indicated on the autoradiograph (right). Darker areas of autoradiograph (right) are a result of increased radioactivity due to higher Pu concentration.

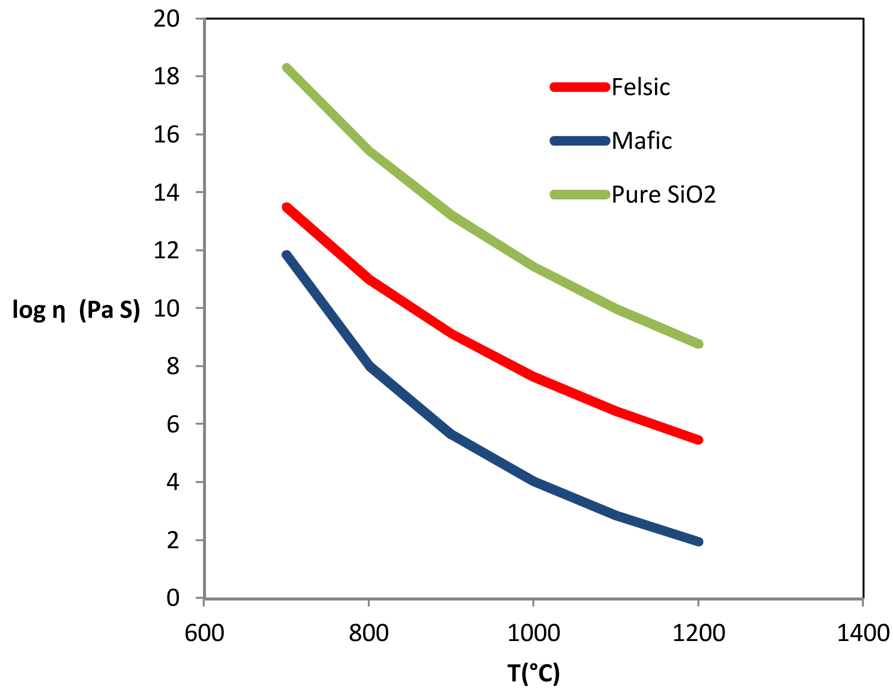

Figure 12: Viscosity as a function of temperature for the majority endmember compositions of SiO_2, felsic, and mafic glass.

Conclusions:

This study demonstrated that it is possible to combine mapping of major element composition to plutonium mapping by autoradiography in order to gain a better understanding of plutonium segregation in fallout, and the relationship between plutonium and the primary constituents of fallout glasses. It was found that this sample set of fallout could be described with a small number of endmember compositions. Furthermore, it was shown that plutonium was most strongly associated with the mafic glass endmember composition and excluded from the pure endmember compositions of felsic glass, SiO_2, and inclusionary phases. This may explain previous observations of plutonium correlation with the elements calcium and iron and the anti-correlation with potassium and sodium in trinitite.[29] In light of this study, it may be concluded that this is a correlation with a mafic glass endmember, but that the relationship with Ca and Fe may not apply when the Ca and Fe are from a different source. This study establishes a correlation with the mafic glass composition and an anti-correlation with felsic glass, SiO_2, and inclusion-like endmembers, and emphasizes that it is likely the characteristics of the endmember composition as opposed to the chemical characteristics of the individual elements that drive this behavior. Viscosity may be a determining factor for plutonium incorporation into nuclear fallout melt glasses. The lower viscosity of the mafic glass may permit more plutonium inclusion through greater mixing, but this supposition requires further investigation.

Acknowledgements:
This work has been supported by the Defense Threat Reduction Agency (DTRA) under contract DTRA10027-10788 at LLNL and under contract HDTRA1412237 at AFIT. This work was supported by the NNSA Office of Defense Nuclear Nonproliferation R&D (NA-22) of the U.S. Department of Energy. This support does not constitute an express or implied endorsement on the part of the Government. This work was performed under the auspices of the U.S. DOE by Lawrence Livermore National Laboratory under contract DE-AC52-07NA27344.

References:

[1]S. Glasstone and P.J. Dolan *The Effects of Nuclear Weapons* United States Department of Defense and the Energy Research and Development Administration, Washington D.C. 1977.

[2]C.F. Miller *Biological and Radiological Effects of Fallout from Nuclear Explosions* Stanford Research Institute, Menlo Park USA 1964.

[3]G.R. Crocker, J.D. O'Conner and E.C. Freiling *Physical and Radiochemical Properties of Fallout Particles* 1965, Technical Report USNRDL-TR-899.

[4]E.C. Freiling, *Science,* 1961, **133**, 1991.

[5]E.C. Freiling and N.E. Ballou, *Nature,* 1962, **195**, 1283.

[6]K. Edvarson, K. Löw and J. Sisefsky, *Nature,* 1959, **184**, 1771.

[7]D. Weisz, B. Jacobsen, N.E. Marks, K.B. Knight, B.H. Isselhardt, J.E. Matzel, S.G. Prussin, I.D. Hutcheon, *Geochim. Et Cosmochim. Ac.*, in press.

[8]H.A. Tewes, *Nucl. Appl. Technol.,* 1969, 7, 232.

[9]J. Sisefsky, *Science,* 1961, **133**, 735.

[10]R.W. Taylor, E.L. Lee and J.H. Hill, *Proceedings of the Symposium Engineering with Nuclear Explosives,* CONF-700101, 1970, **1**, 794.

[11]J.M Kelley, L.A. Bond and T.M. Beasley, *Sci. Total Environ.,* 1999, ***237/238***, 483.

[12]S.M. Bowen, D.L. Finnegan, J.L. Thompson, C.M. Miller, P.L. Baca, L.F. Olivas, C.G. Geoffrion, D.K. Smith, W. Goishi, B.K. Esser, J.W. Meadows, N. Namboodiri and J.F. Wild, *Nevada Test Site Radionuclide Inventory 1951-1992,* 2001, Technical Report LA-13859-MS.

[13] IAEA, Radiological Conditions at the Former French Nuclear Test Sites in Algeria: Preliminary Assessment and Recommendations, In: *Radiological Assessment reports Series.* International Atomic Energy Agency, Vienna.

[14] M. Yamamoto, T. Tsukatani and T.Y. Katayama, *Health Phys.,* 1996, **71**, 142.

[15] *United States Nuclear Tests, July 1945 through September 1992*, DOE/NV-209 Rev 15, United States Department of Energy Nevada Operations Office, Las Vegas NV USA, 2000.

[16] I.Y. Borg, *Nucl. Technol.,* 1974, **26**, 88.

[17] C.E. Adams and J.D. O'Connor, *Research and Development Technical Report*, USNRDL-TR-208, 1957.

[18] F. Belloni, J. Himbert, O. Marzocchi and V. Romanello, *J. Environ. Radioactiv.,* 2011, **102**, 852.

[19] A.J. Fahey, C.J. Zeissler, D.E. Newbury, J. Davis and R.M. Lindstrom, *P. Natl. Acad. Sci.,* 2010, **107**, 20207.

[20] R.E. Hermes and W.B. Strickfaden, *Nuclear Weapons Journal,* 2005, **2**, 2.

[21] C.E. Adams, N.H. Farlow and W.R. Schell, *Geochim. Cosmochim. Ac.,* 1960, **18**, 42.

[22] J. Mackin, P. Zigman, D. Love, D. Macdonald and D. Sam, *J. Inorg. Chem.,* 1960, **15**, 20.

[23] R.C. Gostic, K.B. Knight, G.D. Spriggs and I.D. Hutcheon, presented at *Pacifichem 2010, International Chemical Congress of Pacific Basin Societies,* Honolulu, HI, USA, December 15-20, 2010.

[24] G.R. Eppich, K.B. Knight, T.W. Jacomb-Hood, G.D. Spriggs and I.D. Hutcheon, *J. Radioanal. Nucl. Chem.,* 2014, **302**, 593.

[25] L.A. Lewis, K.B. Knight, J.E. Matzel, S.G. Prussin, M.M. Zimmer, W.S. Kinman, F.J. Ryerson and I.D. Hutcheon, *J. Environ. Radioactiv.,* 2015, **148**, 183.

[26] W.S. Cassata, S.G. Prussin, K.B. Knight, I.D. Hutcheon, B.H. Isselhardt and P.R. Renne, *J. Environ. Radioactiv.,* 2014, **137**, 88.

[27] J.J. Bellucci, A. Simonetti, C. Wallace, E.C. Koeman and P.C. Burns, *Anal. Chem.,* 2013, **85**, 7588.

[28] E.C. Koeman, A. Simonetti and P.C. Burns, *Anal. Chem.,* 2015, **87**, 5380.

[29] C. Wallace, J.J. Bellucci, A. Simonetti, T. Hainley, E.C. Koeman and P.C. Burns, *J. Radioanal. Nucl. Chem.,* 2013, **298**, 993.

[30]J.J. Bellucci, A. Simonetti, C. Wallace, E.C. Koeman and P.C. Burns, *Anal. Chem.,* 2013, **85**, 4195.

[31]T. Parsons-Moss, K. Knight, M. Fitzgerald, G. Stone, L. Caldeira, M. Kristo, unpublished work.

[32]M.D. Abramoff, P.J. Magalhaes and S.J. Ram, *Biophotonics International,* 2004, **11**, 36.

[33]G.A. Gualda, M.S. Ghiorso, R.V. Lemons and T.L. Carley, *J. Petrol.,* 2012, **53**, 875.

[34]K. Stewart, *Trans. Faraday Soc.,* 1956, **52**, 161.

Supplemental Information

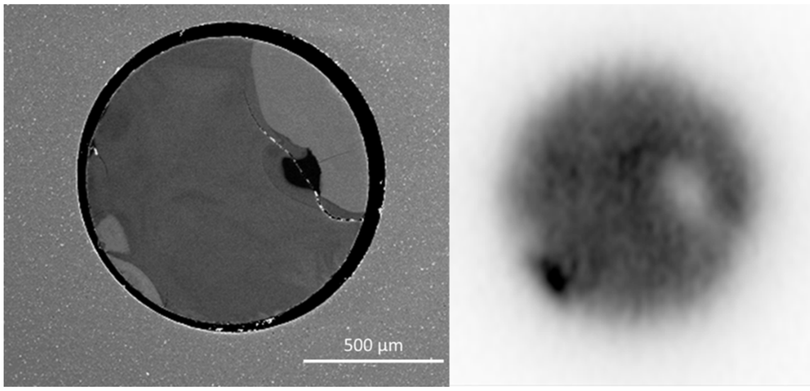

SI Figure 1: Backscattered electron image of sample 1 from expanded study (left) and autoradiography (right).

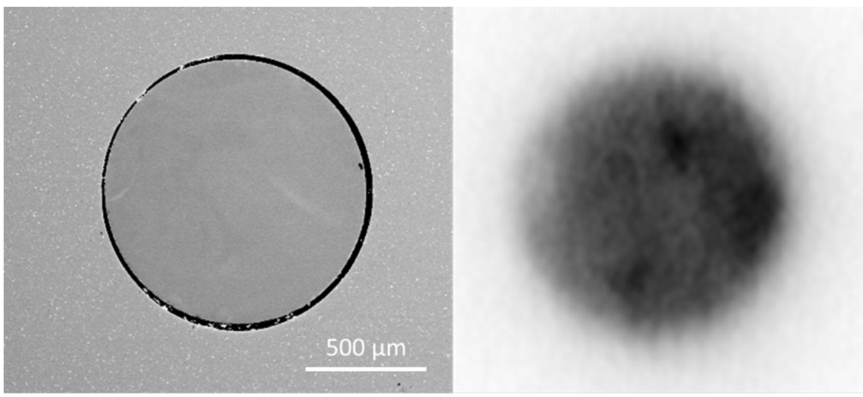

SI Figure 2: Backscattered electron image of sample 2 from expanded study (left) and autoradiography (right).

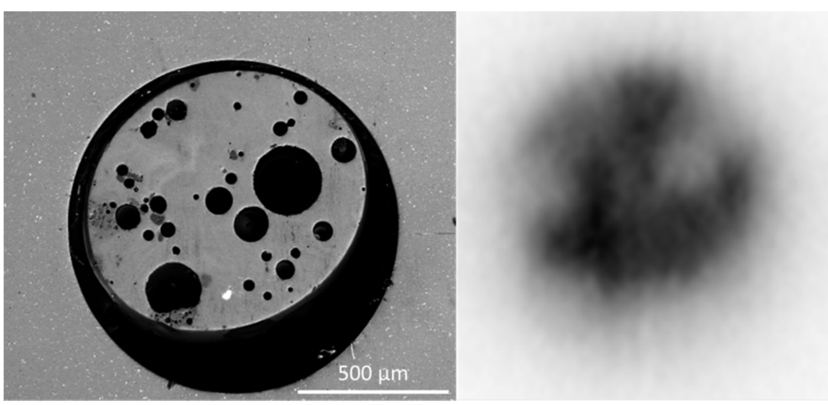

SI Figure 3: Backscattered electron image of sample 3 from expanded study (left) and autoradiography (right).

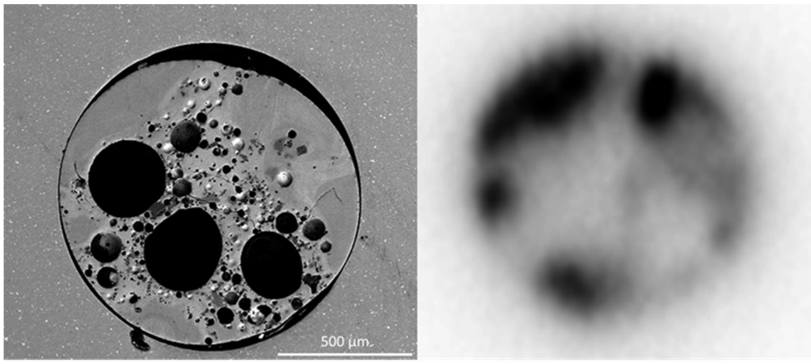

SI Figure 4: Backscattered electron image of sample 4 from expanded study (left) and autoradiography (right).

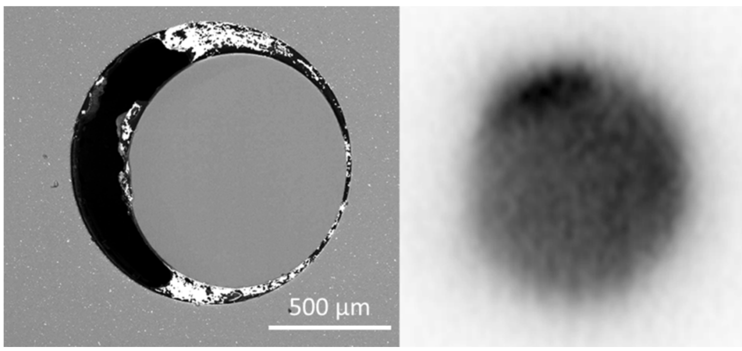

SI Figure 5: Backscattered electron image of sample 5 from expanded study (left) and autoradiography (right).

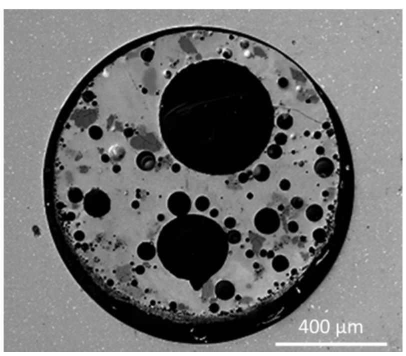

SI Figure 6: Backscattered electron image of sample 6 from expanded study. No activity registered in autoradiography.

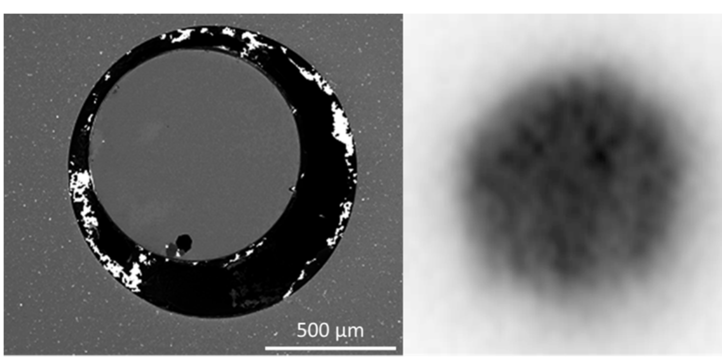

SI Figure 7: Backscattered electron image of sample 7 from expanded study (left) and autoradiography (right).

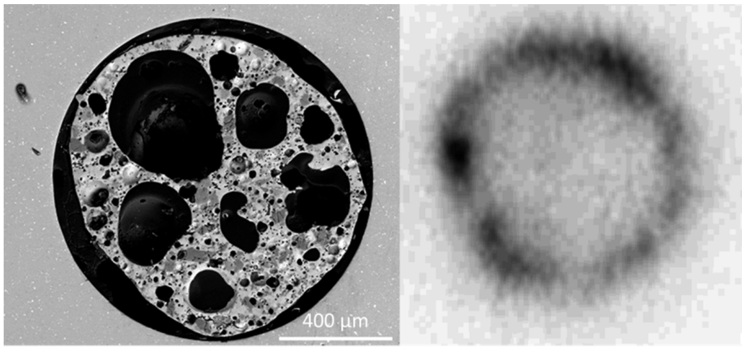

SI Figure 8: Backscattered electron image of sample 8 from expanded study (left) and autoradiography (right).

*Sample 9 lost in sample preparation.

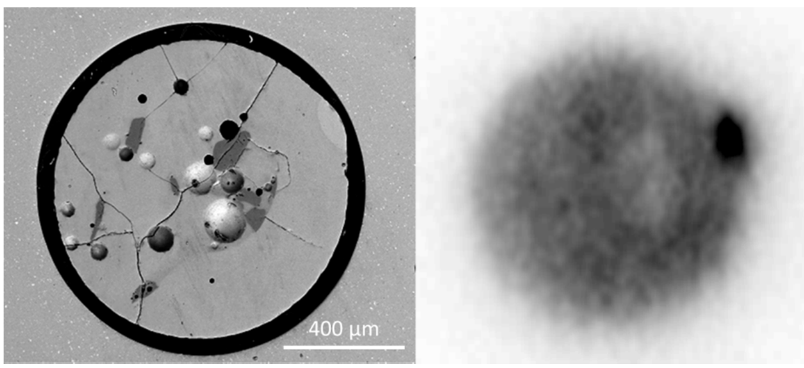

SI Figure 9: Backscattered electron image of sample 10 from expanded study (left) and autoradiography (right).

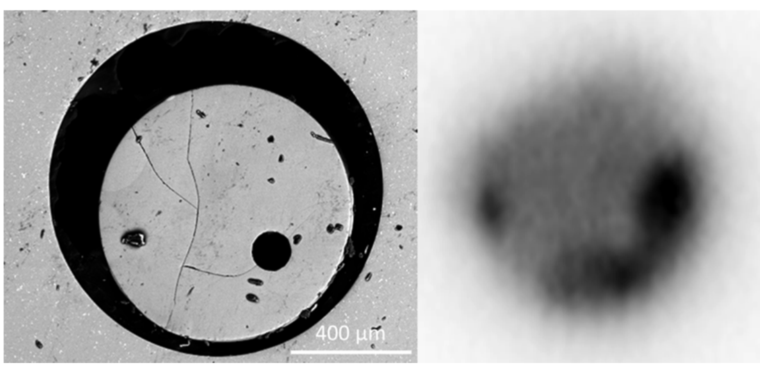

SI Figure 10: Backscattered electron image of sample 11 from expanded study (left) and autoradiography (right). Irregular particles are surface contamination, while nearly perfect circle is a vesicle.

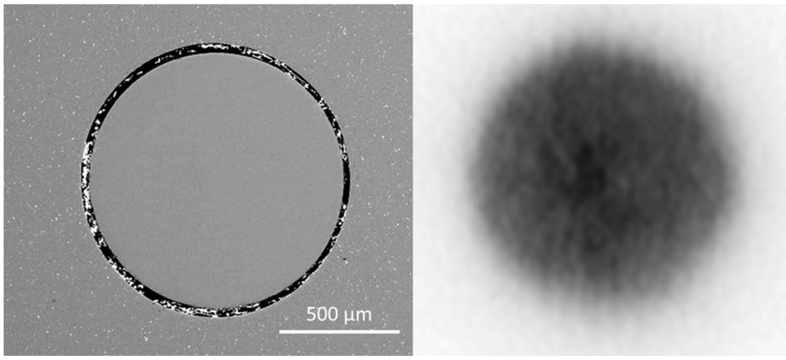

SI Figure 11: Backscattered electron image of sample 12 from expanded study (left) and autoradiography (right).

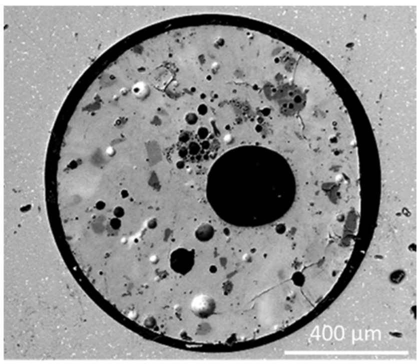

SI Figure 12: Backscattered electron image of sample 13 from expanded study. No activity registered in autoradiography.

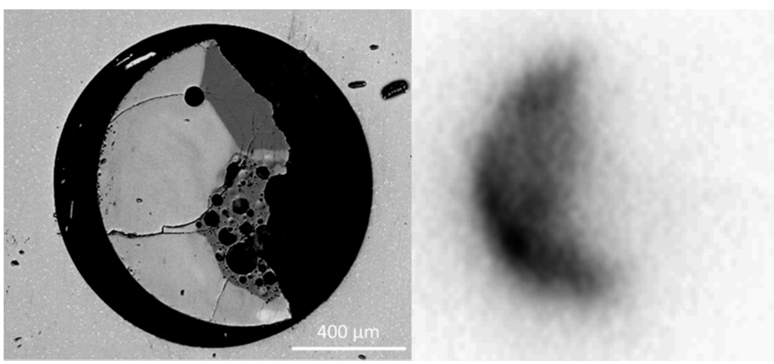

SI Figure 13: Backscattered electron image of sample 14 from expanded study (left) and autoradiography (right).

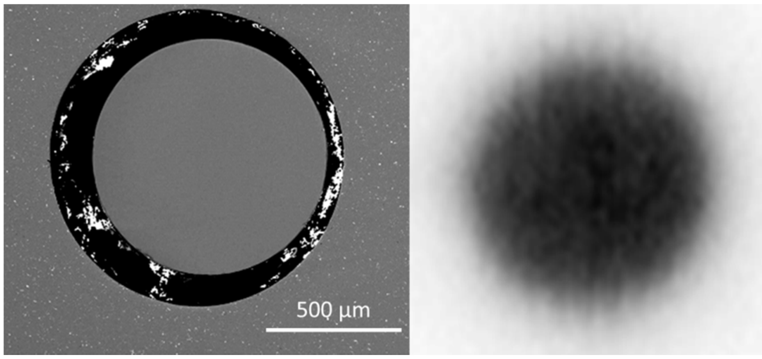

SI Figure 14: Backscattered electron image of sample 15 from expanded study (left) and autoradiography (right).

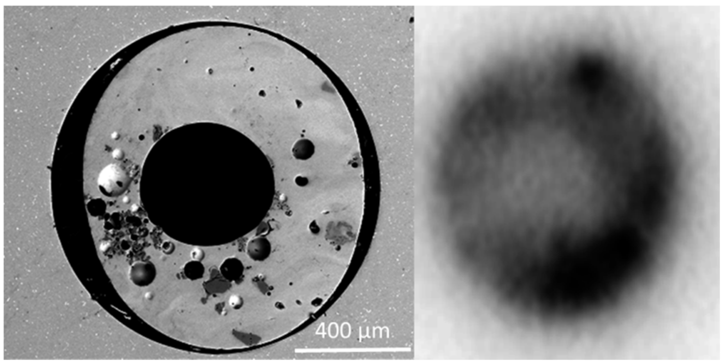

SI Figure 15: Backscattered electron image of sample 16 from expanded study (left) and autoradiography (right).

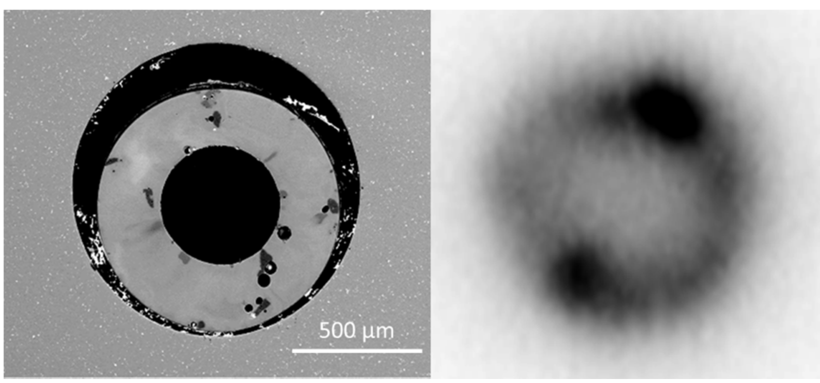

SI Figure 16: Backscattered electron image of sample 17 from expanded study (left) and autoradiography (right).

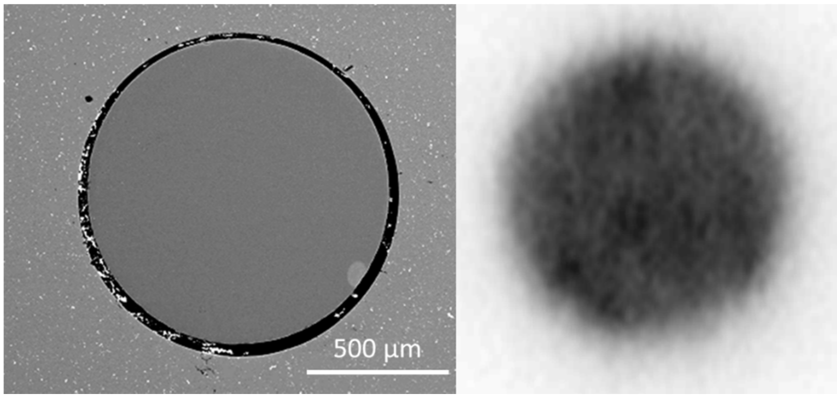

SI Figure 17: Backscattered electron image of sample 18 from expanded study (left) and autoradiography (right).

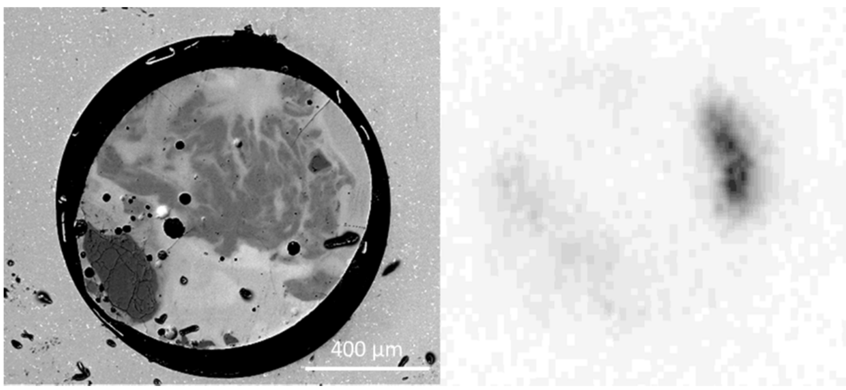

SI Figure 18: Backscattered electron image of sample 19 from expanded study (left) and autoradiography (right).

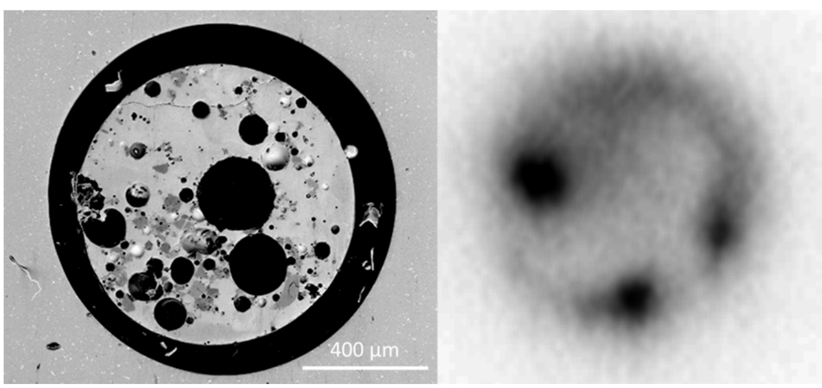

SI Figure 19: Backscattered electron image of sample 20 from expanded study (left) and autoradiography (right).

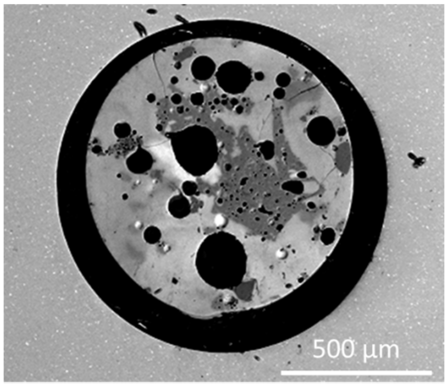

SI Figure 20: Backscattered electron image of sample 21 from expanded study (left). There was no activity by autoradiography.

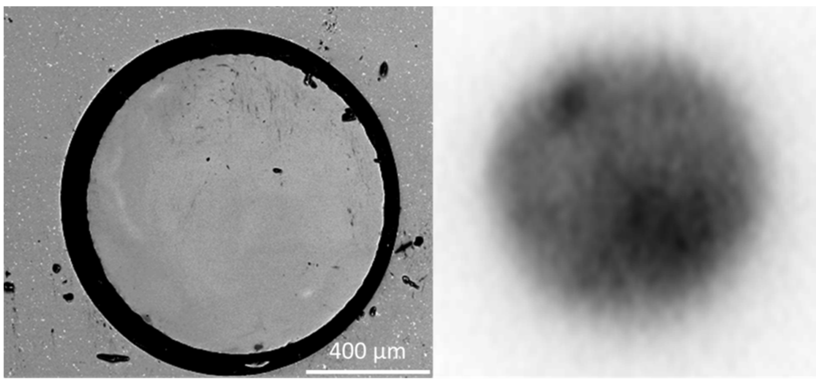

SI Figure 21: Backscattered electron image of sample 22 from expanded study (left) and autoradiography (right).

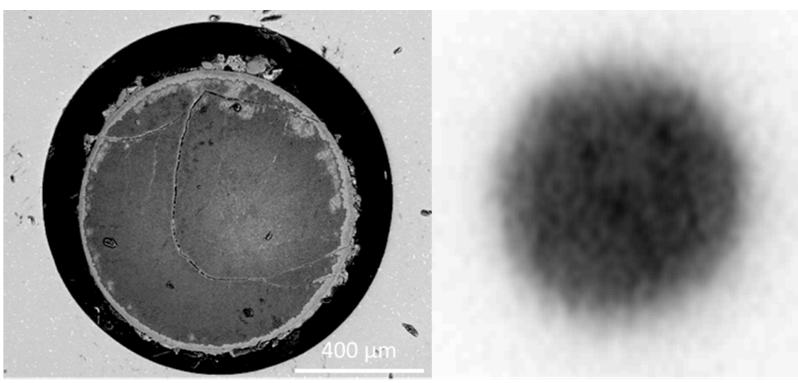

SI Figure 22: Backscattered electron image of sample 23 from expanded study (left) and autoradiography (right).

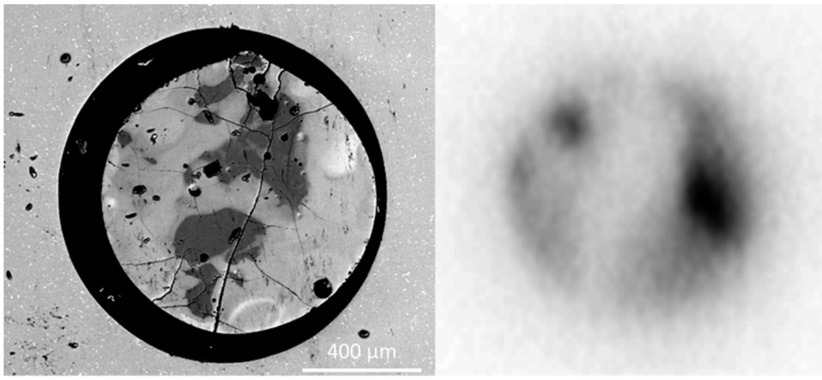

SI Figure 23: Backscattered electron image of sample 24 from expanded study (left) and autoradiography (right).

*Sample 25 lost in sample preparation.

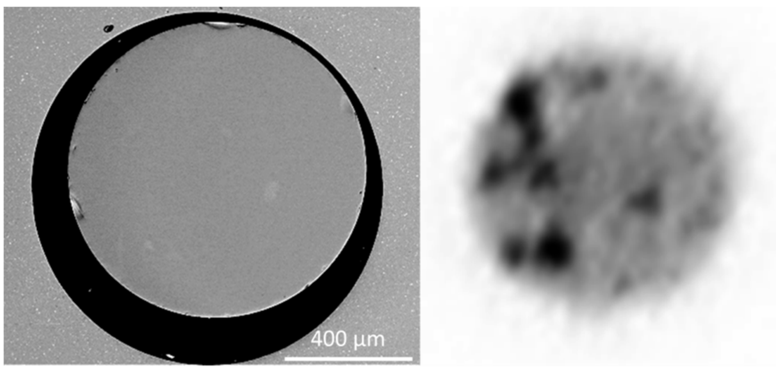

SI Figure 24: Backscattered electron image of sample 26 from expanded study (left) and autoradiography (right).

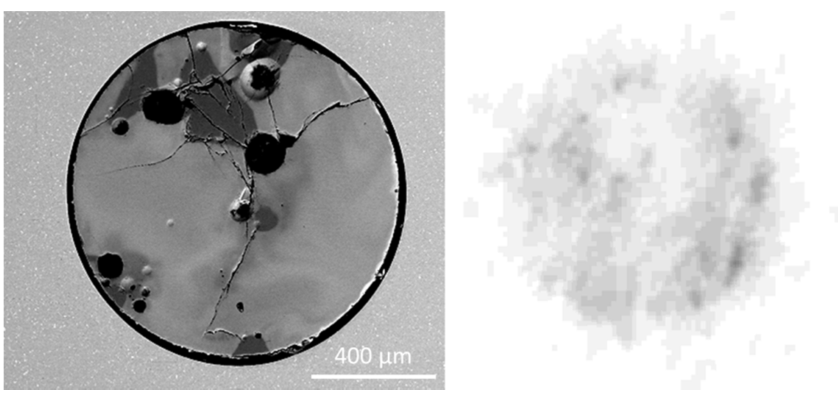

SI Figure 25: Backscattered electron image of sample 27 from expanded study (left) and autoradiography (right).

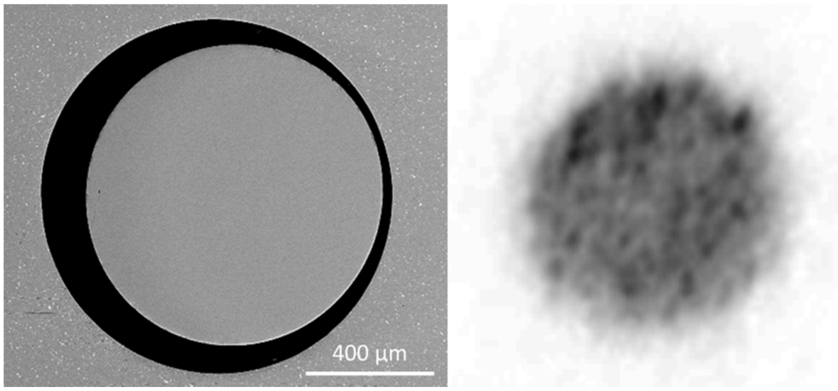

SI Figure 26: Backscattered electron image of sample 28 from expanded study (left) and autoradiography (right).

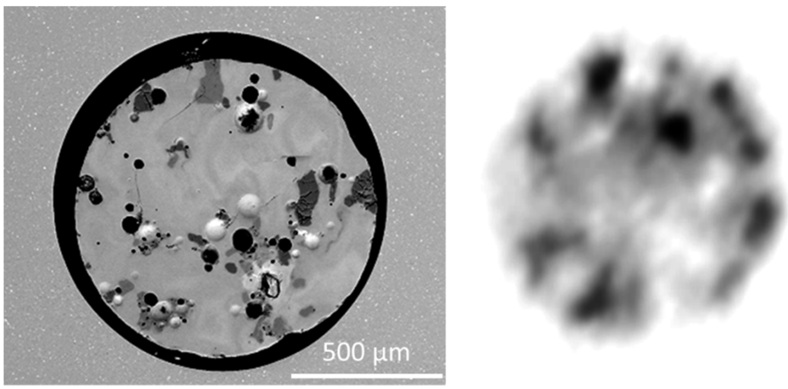

SI Figure 27: Backscattered electron image of sample 29 from expanded study (left) and autoradiography (right).

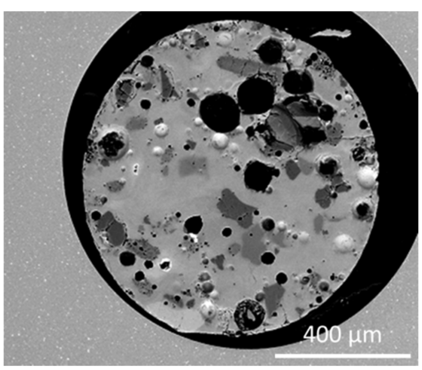

SI Figure 28: Backscattered electron image of sample 30 from expanded study (left). No activity was present in autoradiography.

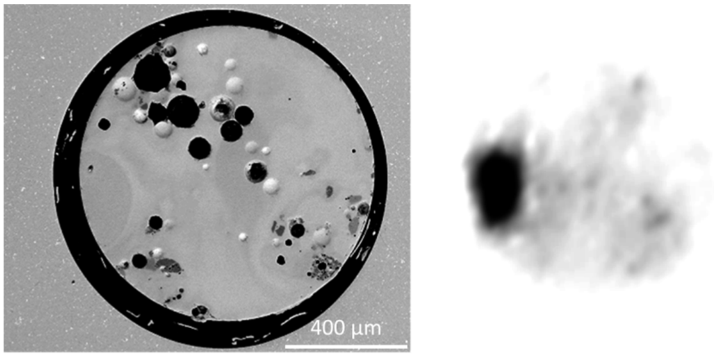

SI Figure 29: Backscattered electron image of sample 31 from expanded study (left) and autoradiography (right).

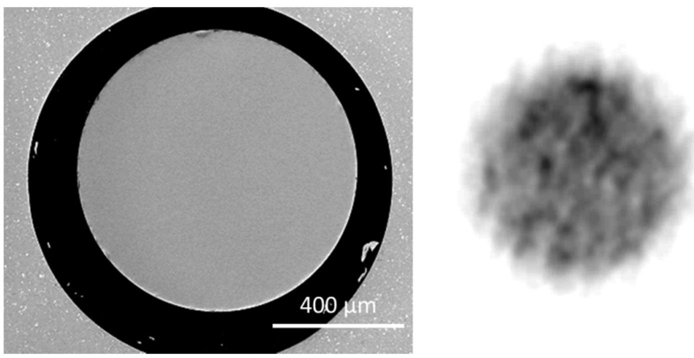

SI Figure 30: Backscattered electron image of sample 32 from expanded study (left) and autoradiography (right).

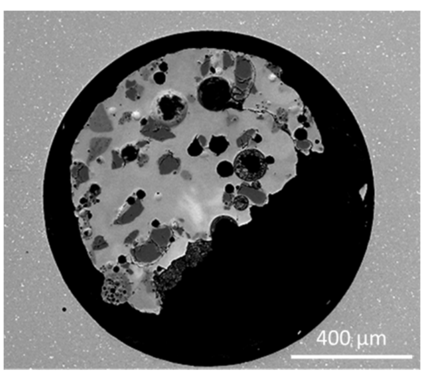

SI Figure 31: Backscattered electron image of sample 33 from expanded study (left). No activity was present in autoradiography.

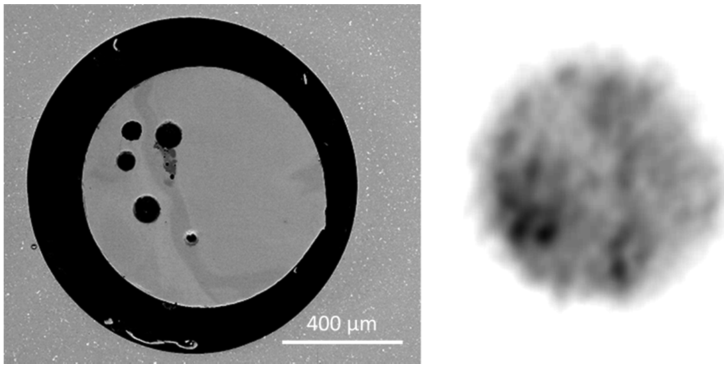

SI Figure 32: Backscattered electron image of sample 34 from expanded study (left) and autoradiography (right).

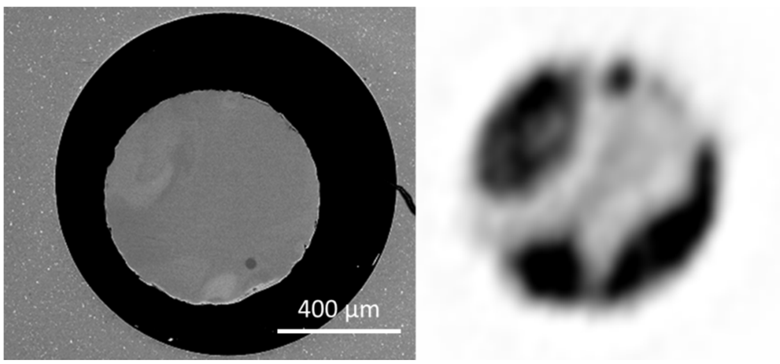

SI Figure 33: Backscattered electron image of sample 35 from expanded study (left) and autoradiography (right).

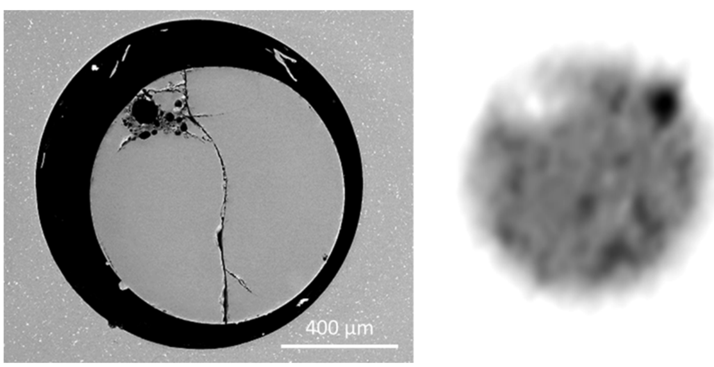

SI Figure 34: Backscattered electron image of sample 36 from expanded study (left) and autoradiography (right).

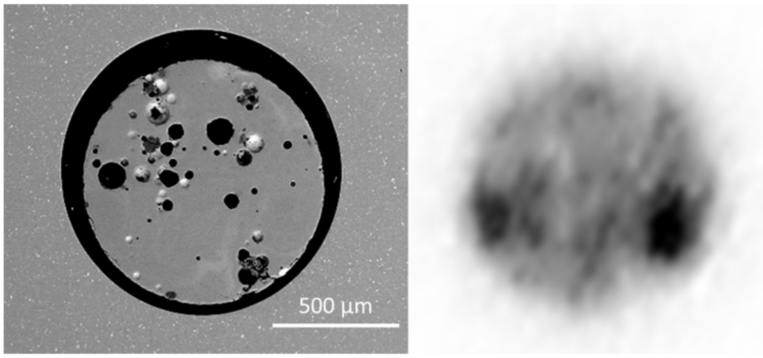

SI Figure 35: Backscattered electron image of sample 37 from expanded study (left) and autoradiography (right).

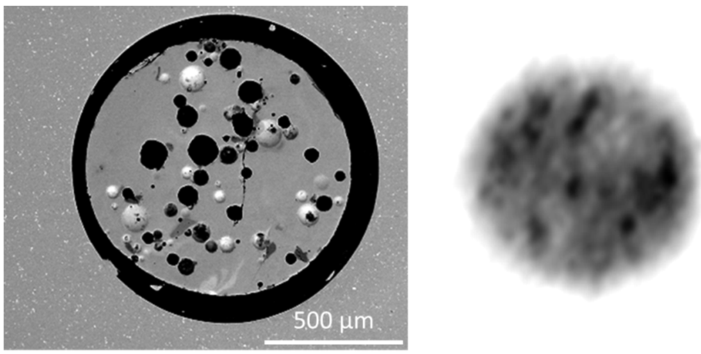

SI Figure 36: Backscattered electron image of sample 38 from expanded study (left) and autoradiography (right).

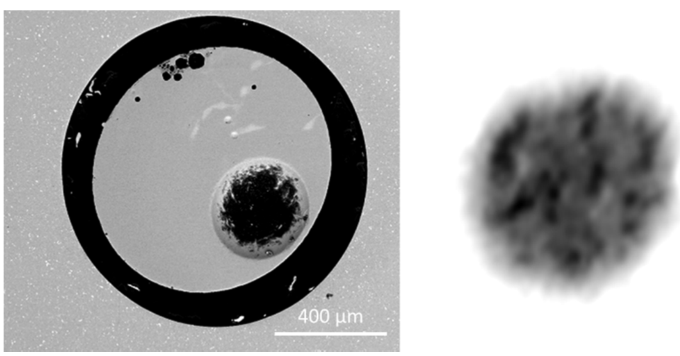

SI Figure 37: Backscattered electron image of sample 39 from expanded study (left) and autoradiography (right).

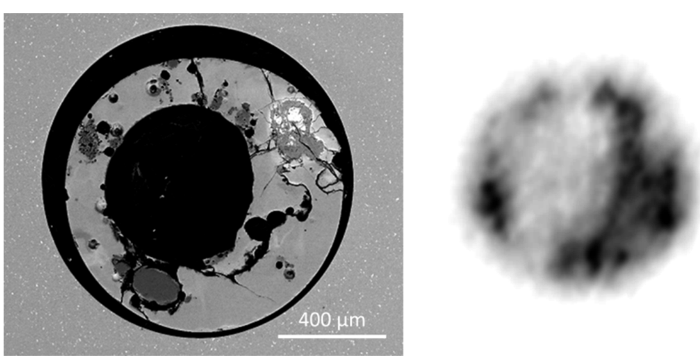

SI Figure 38: Backscattered electron image of sample 40 from expanded study (left) and autoradiography (right).

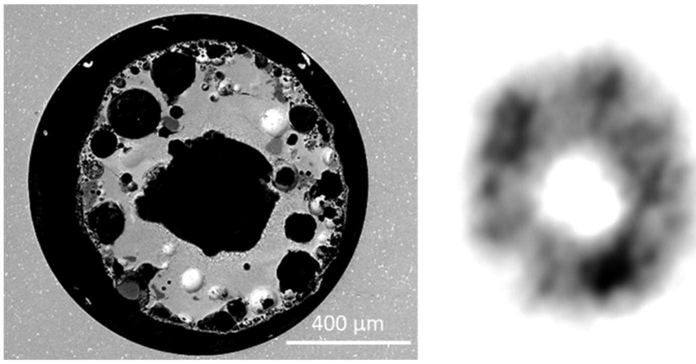

Figure 39: Backscattered electron image of sample 41 from expanded study (left) and autoradiography (right).

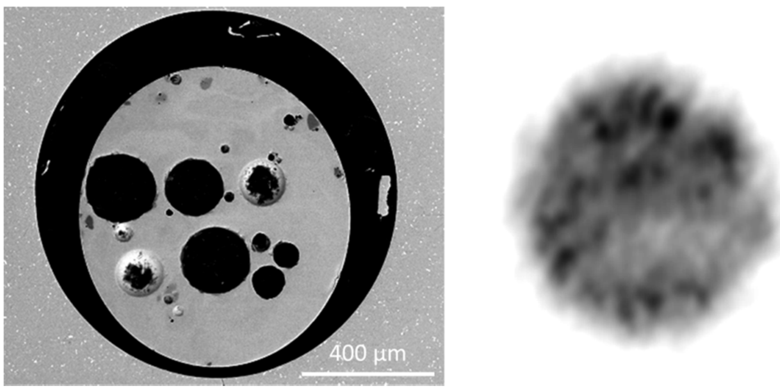

SI Figure 40: Backscattered electron image of sample 42 from expanded study (left) and autoradiography (right).

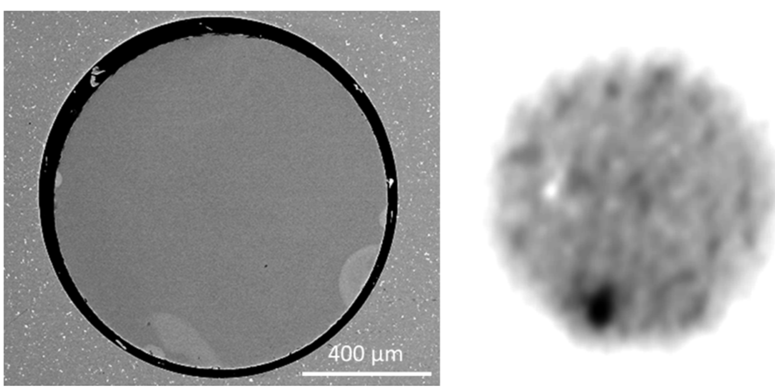

SI Figure 41: Backscattered electron image of sample 43 from expanded study (left) and autoradiography (right).

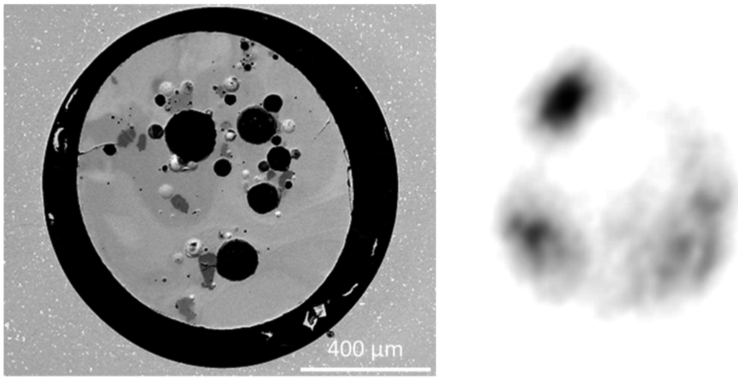

SI Figure 42: Backscattered electron image of sample 44 from expanded study (left) and autoradiography (right).

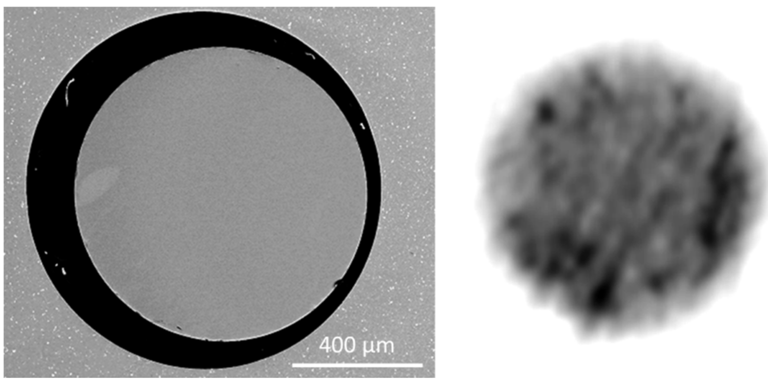

SI Figure 43: Backscattered electron image of sample 45 from expanded study (left) and autoradiography (right).

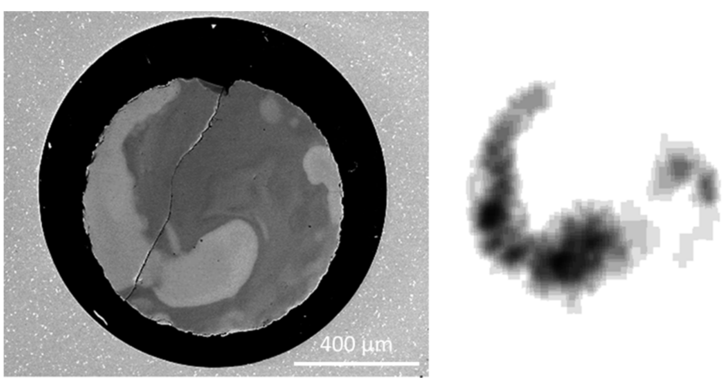

SI Figure 44: Backscattered electron image of sample 46 from expanded study (left) and autoradiography (right).

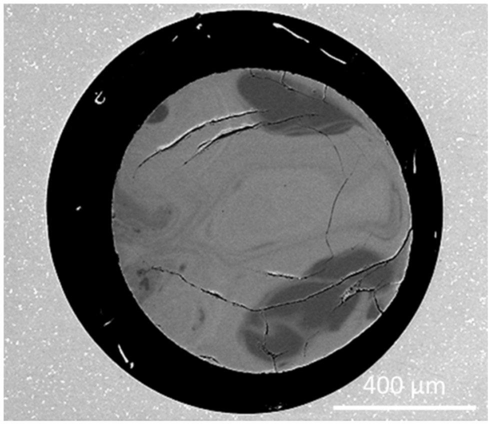

SI Figure 45: Backscattered electron image of sample 47 from expanded study (left). No activity was present in autoradiography.

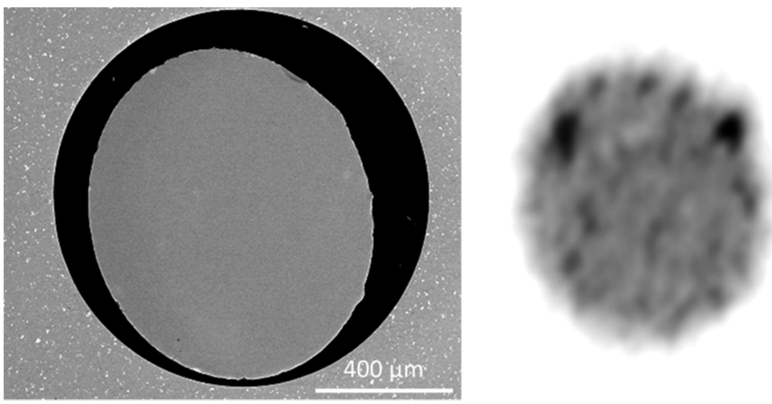

SI Figure 46: Backscattered electron image of sample 48 from expanded study (left) and autoradiography (right).

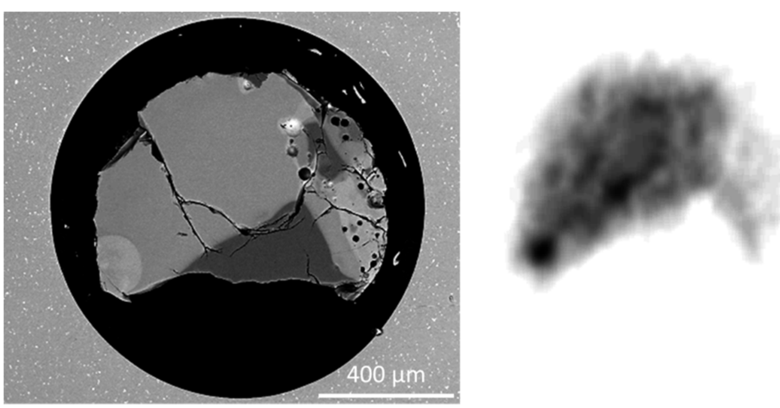

SI Figure 47: Backscattered electron image of sample 49 from expanded study (left) and autoradiography (right).

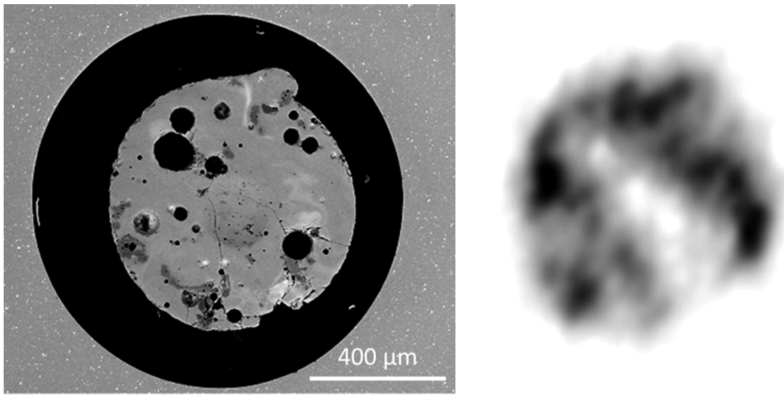

SI Figure 48: Backscattered electron image of sample 50 from expanded study (left) and autoradiography (right).

Table 1: Quantification of each endmember by thresholding of the backscattered electron image.

Sample #	homogeneous	Pore Space	Mafic Glass	SiO2	Felsic Glass	other inclusions
1	0	0	98	1.8	0	0
2	100	0	0	0	0	0
3	0	22	72	1.6	2.8	0.82
4	0	30	64	4.7	0	0
5	100	0	0	0	0	0
6	0	36	56	5.5	8.3	1.2
7	98	0.83	0	1.5	0	0
8	0	54	29	11	7	0
10	90	3.3	4.4	5.9	0	0
11	98	2.4	0	0	0	0
12	100	0	0	0	0	0
13	0	13	84	5.4	7.8	0.5
14	0	8.4	63	17	12	0
15	100	0	0	0	0	0
16	0	23	73	4.2	4.5	0
17	0	25	71	3.6	0	0
18	100	0	0	0	0	0
19	41	3.5	47	8.5	0	0
20	0	27	60	13	0	0
21	0	18	57	5.2	22	0
22	100	0	0	0	0	0
23	100	0	0	0	0	0
24	0	2.2	66	22	0	1.5
26	100	0	0	0	0	0
27	0	7.8	82	11	0	0
28	100	0	0	0	0	0
29	0	6.8	74	11	7	3.2
30	0	14	59	20	7.9	1.2
31	0	7	89	1.6	3	0
32	100	0	0	0	0	0
33	0	12	71	11	12	1.5
34	0	3.7	94	1.9	0	0
35	100	0	0	0	0	0
36	0	2.5	94	3.1	0	0
37	0	6.9	87	3.4	2.9	0.1
38	0	12	81	8.9	0	0
39	0	12	84	4.5	0	0
40	0	40	48	4.5	5.7	1.6
41	0	40	48	11.6	0	0
42	0	20	76	4.8	0	0
43	100	0	0	0	0	0
44	0	13	80	3	4.1	0
45	100	0	0	0	0	0
48	100	0	0	0	0	0
49	0	4.3	76	19	0	0
50	0	13	77	7.5	0	1.4
min	0	0	0	0	0	0
max	100	54	98	22	22	3.2
average	37.5	10.5	44.9	5.2	2.3	0.3
heterogeneous		16.9	71.9	7.9	3.8	0.5
heterogeneous no vessicle			85.5	9.4	4.5	0.6

Table 2: Semi-quantitative point analysis by energy dispersive spectroscopy (typical error is 2-3% 1 sigma). Elements associated with conductive coating and anions such as oxygen are not reported. Elements are normalized to 100% and assumed to exist as oxides. Samples 3, 6, 8, 11, and 13 were randomly chosen for other analysis and are not reported here.

Sample #	Area #	Point #	Si	Ca	Mg	Al	K	Na	Fe	Ti	Zr	Mn
1	1	1	48.3	23.7	9.2	15.8	0.0	0.0	3.0	0.0	0.0	0.0
1	1	2	48.5	22.3	9.0	16.1	1.5	0.0	2.6	0.0	0.0	0.0
1	1	3	100.0	0.0	0.0	0.0	0.0	0.0	0.0	0.0	0.0	0.0
1	1	4	46.5	25.1	7.6	18.2	0.0	0.0	2.6	0.0	0.0	0.0
1	1	5	47.6	24.9	7.5	14.1	3.0	0.0	2.9	0.0	0.0	0.0
1	1	6	47.3	13.2	1.5	21.6	13.1	0.0	3.4	0.0	0.0	0.0
1	1	7	55.8	19.8	5.8	16.6	0.0	0.0	2.0	0.0	0.0	0.0
1	1	8	55.2	19.7	6.5	16.4	0.0	0.0	2.1	0.0	0.0	0.0
1	1	9	53.7	19.8	5.8	18.8	0.0	0.0	1.8	0.0	0.0	0.0
1	1	10	51.3	20.0	6.0	20.9	0.0	0.0	1.9	0.0	0.0	0.0
2	1	1	48.3	24.3	7.9	13.7	1.9	0.0	4.0	0.0	0.0	0.0
2	1	2	53.8	22.1	5.7	13.3	3.5	0.0	1.6	0.0	0.0	0.0
2	1	3	51.2	21.9	7.4	14.3	2.1	0.0	3.2	0.0	0.0	0.0
2	1	4	53.7	21.3	5.8	14.1	3.4	0.0	1.6	0.0	0.0	0.0
2	1	5	52.4	19.1	5.2	14.8	3.9	3.1	1.4	0.0	0.0	0.0
2	1	6	51.2	19.8	6.2	14.1	3.5	3.7	1.6	0.0	0.0	0.0
2	1	7	52.0	22.4	6.4	14.1	3.3	0.0	1.7	0.0	0.0	0.0
2	1	8	52.5	20.1	5.4	13.8	3.7	3.0	1.6	0.0	0.0	0.0
2	1	9	50.5	21.5	6.3	13.6	3.4	2.9	1.7	0.0	0.0	0.0
2	1	10	53.3	21.5	6.0	13.9	3.5	0.0	1.8	0.0	0.0	0.0
2	1	11	52.3	21.6	6.1	14.7	3.8	0.0	1.5	0.0	0.0	0.0
4	1	1	46.7	24.2	8.9	15.2	2.6	0.0	2.5	0.0	0.0	0.0
4	1	2	42.9	26.3	9.3	14.9	3.2	0.0	3.5	0.0	0.0	0.0
4	1	3	45.9	23.7	8.2	15.6	4.0	0.0	2.6	0.0	0.0	0.0
4	1	4	46.8	21.9	7.8	13.4	4.6	3.1	2.5	0.0	0.0	0.0
4	1	5	48.0	19.5	7.8	11.9	5.9	4.1	2.7	0.0	0.0	0.0
4	1	6	47.1	24.6	8.4	15.4	1.9	0.0	2.6	0.0	0.0	0.0
4	1	7	45.6	25.6	8.7	15.9	1.7	0.0	2.5	0.0	0.0	0.0
4	1	8	35.8	34.0	7.7	20.6	0.0	0.0	1.9	0.0	0.0	0.0
4	1	9	47.4	25.2	8.2	14.7	2.2	0.0	2.3	0.0	0.0	0.0
4	1	10	39.9	29.9	8.8	19.1	0.0	0.0	2.3	0.0	0.0	0.0
4	1	11	46.5	24.8	8.8	15.4	1.9	0.0	2.6	0.0	0.0	0.0
4	1	12	46.4	25.9	8.7	16.3	0.0	0.0	2.8	0.0	0.0	0.0
4	1	13	47.2	25.7	8.6	15.7	0.0	0.0	2.7	0.0	0.0	0.0
4	1	14	46.4	26.5	7.5	15.2	1.9	0.0	2.6	0.0	0.0	0.0
4	1	15	40.3	30.8	10.4	13.7	1.4	0.0	3.4	0.0	0.0	0.0
5	1	1	52.2	21.1	7.6	16.6	0.0	0.0	2.5	0.0	0.0	0.0
5	1	2	50.0	24.0	7.2	16.2	0.0	0.0	2.5	0.0	0.0	0.0
5	1	3	49.5	24.9	7.8	14.8	0.0	0.0	3.0	0.0	0.0	0.0
5	1	4	49.2	24.5	8.1	15.2	0.0	0.0	2.9	0.0	0.0	0.0
5	1	5	49.1	22.9	8.7	15.0	1.7	0.0	2.6	0.0	0.0	0.0
5	1	6	49.5	23.5	8.3	16.0	0.0	0.0	2.6	0.0	0.0	0.0
5	1	7	49.4	24.4	8.0	15.2	0.0	0.0	2.9	0.0	0.0	0.0
5	1	8	49.0	24.7	8.3	15.2	0.0	0.0	2.8	0.0	0.0	0.0
5	1	9	49.2	24.4	8.2	15.3	0.0	0.0	2.9	0.0	0.0	0.0
5	1	10	49.5	24.2	8.3	15.3	0.0	0.0	2.8	0.0	0.0	0.0
7	1	1	40.1	25.1	1.3	15.4	10.2	0.0	8.0	0.0	0.0	0.0
7	1	2	0.0	0.0	0.0	100.0	0.0	0.0	0.0	0.0	0.0	0.0
7	1	3	100.0	0.0	0.0	0.0	0.0	0.0	0.0	0.0	0.0	0.0
7	1	4	100.0	0.0	0.0	0.0	0.0	0.0	0.0	0.0	0.0	0.0
7	1	5	46.8	24.3	8.4	15.2	2.6	0.0	2.7	0.0	0.0	0.0
7	1	6	46.5	23.0	9.3	15.6	3.0	0.0	2.7	0.0	0.0	0.0
10	1	1	43.0	31.9	6.4	18.7	0.0	0.0	0.0	0.0	0.0	0.0
10	1	2	42.9	31.8	6.8	18.5	0.0	0.0	0.0	0.0	0.0	0.0

Sample #	Area #	Point #	Si	Ca	Mg	Al	K	Na	Fe	Ti	Zr	Mn
10	1	3	48.6	24.1	8.5	16.0	2.8	0.0	0.0	0.0	0.0	0.0
10	1	4	51.4	21.8	7.1	15.3	4.3	0.0	0.0	0.0	0.0	0.0
10	1	5	50.1	23.6	8.0	15.0	3.3	0.0	0.0	0.0	0.0	0.0
10	1	6	48.7	23.7	8.7	16.1	2.8	0.0	0.0	0.0	0.0	0.0
10	1	7	48.6	24.4	8.2	15.7	3.1	0.0	0.0	0.0	0.0	0.0
10	1	8	48.7	24.1	8.6	15.8	2.8	0.0	0.0	0.0	0.0	0.0
10	1	9	48.3	24.5	8.4	15.9	2.9	0.0	0.0	0.0	0.0	0.0
10	1	10	52.3	20.0	7.4	14.0	3.9	0.0	2.5	0.0	0.0	0.0
10	1	11	50.0	23.4	8.1	15.4	3.2	0.0	0.0	0.0	0.0	0.0
10	1	12	49.2	24.1	8.4	15.3	3.1	0.0	0.0	0.0	0.0	0.0
10	1	13	48.6	24.0	8.0	15.7	3.6	0.0	0.0	0.0	0.0	0.0
10	2	1	42.7	30.5	6.7	18.3	0.0	0.0	1.8	0.0	0.0	0.0
10	2	2	43.2	26.1	8.4	22.4	0.0	0.0	0.0	0.0	0.0	0.0
10	2	3	32.6	26.3	9.7	23.5	0.0	7.9	0.0	0.0	0.0	0.0
10	2	4	42.5	25.5	9.3	22.8	0.0	0.0	0.0	0.0	0.0	0.0
10	2	5	43.4	28.2	8.2	20.2	0.0	0.0	0.0	0.0	0.0	0.0
10	2	6	42.9	25.6	8.3	23.2	0.0	0.0	0.0	0.0	0.0	0.0
10	2	7	46.9	20.9	9.4	18.6	2.4	0.0	1.7	0.0	0.0	0.0
10	2	8	41.3	31.5	6.0	19.4	0.0	0.0	1.8	0.0	0.0	0.0
12	1	1	41.4	28.6	14.8	13.2	0.0	0.0	2.0	0.0	0.0	0.0
12	1	2	41.0	30.0	13.9	12.7	0.0	0.0	2.4	0.0	0.0	0.0
12	1	3	38.4	31.6	14.9	13.1	0.0	0.0	2.0	0.0	0.0	0.0
12	1	4	38.3	30.8	15.5	13.3	0.0	0.0	2.1	0.0	0.0	0.0
12	1	5	39.7	29.7	15.3	13.3	0.0	0.0	2.0	0.0	0.0	0.0
12	1	6	39.7	29.6	15.3	13.2	0.0	0.0	2.1	0.0	0.0	0.0
12	1	7	38.3	31.3	15.4	13.0	0.0	0.0	2.0	0.0	0.0	0.0
12	1	8	38.9	30.9	15.2	12.9	0.0	0.0	2.2	0.0	0.0	0.0
12	1	9	39.0	30.6	15.2	13.1	0.0	0.0	2.1	0.0	0.0	0.0
12	1	10	37.4	31.0	14.9	14.7	0.0	0.0	1.9	0.0	0.0	0.0
14	1	1	100.0	0.0	0.0	0.0	0.0	0.0	0.0	0.0	0.0	0.0
14	1	2	100.0	0.0	0.0	0.0	0.0	0.0	0.0	0.0	0.0	0.0
14	1	3	50.0	18.2	7.4	14.2	2.7	4.6	2.9	0.0	0.0	0.0
14	1	4	50.8	17.7	6.7	13.9	3.7	5.0	2.2	0.0	0.0	0.0
14	1	5	49.1	20.1	7.4	14.4	3.0	3.5	2.6	0.0	0.0	0.0
14	1	6	43.0	36.3	7.1	11.0	0.0	0.0	2.6	0.0	0.0	0.0
14	1	7	100.0	0.0	0.0	0.0	0.0	0.0	0.0	0.0	0.0	0.0
14	1	8	100.0	0.0	0.0	0.0	0.0	0.0	0.0	0.0	0.0	0.0
14	1	9	60.9	8.3	0.0	16.8	3.6	8.2	2.2	0.0	0.0	0.0
14	1	10	49.9	19.6	7.1	14.0	3.0	3.9	2.5	0.0	0.0	0.0
15	1	1	41.9	29.4	11.1	17.6	0.0	0.0	0.0	0.0	0.0	0.0
15	1	2	41.9	30.6	10.3	17.2	0.0	0.0	0.0	0.0	0.0	0.0
15	1	3	41.5	30.4	10.8	17.3	0.0	0.0	0.0	0.0	0.0	0.0
15	1	4	42.0	27.7	12.2	18.1	0.0	0.0	0.0	0.0	0.0	0.0
15	1	5	41.3	28.8	10.6	16.9	0.0	0.0	2.4	0.0	0.0	0.0
15	1	6	41.7	29.9	11.1	17.4	0.0	0.0	0.0	0.0	0.0	0.0
15	1	7	41.5	30.0	11.0	17.5	0.0	0.0	0.0	0.0	0.0	0.0
15	1	8	41.6	29.9	11.0	17.5	0.0	0.0	0.0	0.0	0.0	0.0
16	1	1	53.5	4.3	0.0	25.1	8.8	8.3	0.0	0.0	0.0	0.0
16	1	2	40.4	27.8	12.5	14.2	2.2	0.0	2.9	0.0	0.0	0.0
16	1	3	43.1	29.0	10.2	14.9	0.0	0.0	2.9	0.0	0.0	0.0
16	1	4	56.6	8.0	0.0	21.1	5.6	6.5	2.1	0.0	0.0	0.0
16	1	5	100.0	0.0	0.0	0.0	0.0	0.0	0.0	0.0	0.0	0.0
16	1	6	39.1	30.0	9.2	19.2	0.0	0.0	2.4	0.0	0.0	0.0
16	1	7	44.9	25.9	12.0	14.2	0.0	0.0	3.1	0.0	0.0	0.0
16	1	8	37.4	29.4	14.4	14.2	1.4	0.0	3.2	0.0	0.0	0.0

473

Sample #	Area #	Point #	Si	Ca	Mg	Al	K	Na	Fe	Ti	Zr	Mn
16	1	9	46.9	24.6	7.9	13.9	3.5	0.0	3.2	0.0	0.0	0.0
16	1	10	45.8	23.7	8.5	15.1	4.0	0.0	3.0	0.0	0.0	0.0
17	1	1	42.7	28.7	8.0	18.5	0.0	0.0	2.1	0.0	0.0	0.0
17	1	2	48.8	13.5	2.6	22.9	7.8	4.4	0.0	0.0	0.0	0.0
17	1	3	42.9	28.8	9.3	13.5	2.8	0.0	2.7	0.0	0.0	0.0
17	1	4	49.8	10.0	0.0	26.8	5.4	8.0	0.0	0.0	0.0	0.0
17	1	5	45.4	26.2	8.8	14.0	2.6	0.0	3.0	0.0	0.0	0.0
17	1	6	41.5	29.1	11.8	14.6	0.0	0.0	2.9	0.0	0.0	0.0
17	1	7	45.9	27.7	8.0	13.0	2.9	0.0	2.4	0.0	0.0	0.0
17	1	8	45.2	26.6	8.7	13.5	2.9	0.0	3.1	0.0	0.0	0.0
17	1	9	43.6	26.2	9.8	14.8	2.7	0.0	2.9	0.0	0.0	0.0
17	1	10	50.1	19.6	7.3	12.6	4.4	3.2	2.8	0.0	0.0	0.0
17	1	11	36.8	40.8	8.1	11.7	0.0	0.0	2.5	0.0	0.0	0.0
17	1	12	52.0	13.9	4.3	16.2	8.1	3.7	1.9	0.0	0.0	0.0
17	1	13	46.4	24.8	10.9	12.2	3.0	0.0	2.7	0.0	0.0	0.0
17	1	14	59.3	0.0	0.0	21.2	15.1	4.5	0.0	0.0	0.0	0.0
17	1	15	45.1	25.3	8.0	16.4	2.8	0.0	2.3	0.0	0.0	0.0
18	1	1	56.7	21.6	6.0	13.5	0.0	0.0	2.2	0.0	0.0	0.0
18	1	2	58.8	21.1	5.6	12.4	0.0	0.0	2.1	0.0	0.0	0.0
18	1	3	56.0	22.0	6.2	13.5	0.0	0.0	2.3	0.0	0.0	0.0
18	1	4	48.0	29.9	10.7	9.6	0.0	0.0	1.8	0.0	0.0	0.0
18	1	5	55.7	21.9	6.6	13.6	0.0	0.0	2.2	0.0	0.0	0.0
18	1	6	56.2	21.0	6.8	13.8	0.0	0.0	2.2	0.0	0.0	0.0
18	1	7	56.0	22.2	6.2	13.5	0.0	0.0	2.2	0.0	0.0	0.0
18	1	8	56.5	21.5	6.5	13.3	0.0	0.0	2.1	0.0	0.0	0.0
18	1	9	55.8	21.7	6.5	13.5	0.0	0.0	2.5	0.0	0.0	0.0
18	1	10	56.2	22.0	6.2	13.6	0.0	0.0	2.1	0.0	0.0	0.0
18	1	11	56.1	21.6	6.4	13.6	0.0	0.0	2.3	0.0	0.0	0.0
18	1	12	44.7	31.3	13.4	8.7	0.0	0.0	1.9	0.0	0.0	0.0
18	1	13	56.3	21.6	6.3	13.5	0.0	0.0	2.3	0.0	0.0	0.0
18	1	14	56.1	21.7	6.6	13.4	0.0	0.0	2.2	0.0	0.0	0.0
19	1	1	49.9	15.5	7.0	15.3	2.9	5.1	4.3	0.0	0.0	0.0
19	1	2	41.4	22.7	13.0	18.0	0.0	0.0	5.0	0.0	0.0	0.0
19	1	3	46.2	19.8	7.2	21.5	0.0	0.0	5.2	0.0	0.0	0.0
19	1	4	69.0	2.1	0.0	16.4	6.9	5.5	0.0	0.0	0.0	0.0
19	1	5	62.9	3.5	6.2	20.4	6.9	0.0	0.0	0.0	0.0	0.0
19	1	6	100.0	0.0	0.0	0.0	0.0	0.0	0.0	0.0	0.0	0.0
19	1	7	100.0	0.0	0.0	0.0	0.0	0.0	0.0	0.0	0.0	0.0
19	1	8	52.3	18.7	8.0	12.5	2.4	3.8	2.2	0.0	0.0	0.0
19	1	9	100.0	0.0	0.0	0.0	0.0	0.0	0.0	0.0	0.0	0.0
19	1	10	47.8	14.6	5.3	18.2	2.9	5.3	5.8	0.0	0.0	0.0
19	1	11	49.8	20.5	8.0	12.6	1.6	4.5	3.0	0.0	0.0	0.0
19	1	12	58.7	8.3	2.2	17.3	3.7	4.6	5.3	0.0	0.0	0.0
19	1	13	51.7	10.0	5.5	17.6	3.3	6.2	5.7	0.0	0.0	0.0
19	1	14	72.5	0.0	0.0	15.4	7.0	5.2	0.0	0.0	0.0	0.0
19	1	15	53.6	20.8	9.8	11.1	3.1	0.0	1.6	0.0	0.0	0.0
19	1	16	50.4	17.3	7.3	13.9	2.4	4.7	4.0	0.0	0.0	0.0
19	1	17	44.9	22.9	8.7	16.4	0.0	0.0	7.0	0.0	0.0	0.0
20	1	1	48.1	21.3	8.2	14.8	4.8	0.0	2.8	0.0	0.0	0.0
20	1	2	100.0	0.0	0.0	0.0	0.0	0.0	0.0	0.0	0.0	0.0
20	1	3	40.8	31.0	10.0	13.7	1.8	0.0	2.7	0.0	0.0	0.0
20	1	4	42.3	28.5	8.9	14.9	2.3	0.0	3.1	0.0	0.0	0.0
20	1	5	52.5	6.7	0.0	26.4	0.0	14.4	0.0	0.0	0.0	0.0
20	1	6	51.2	22.3	7.7	13.6	2.5	0.0	2.8	0.0	0.0	0.0
20	1	7	41.7	26.8	8.0	15.1	2.1	0.0	4.7	1.5	0.0	0.0

Sample #	Area #	Point #	Si	Ca	Mg	Al	K	Na	Fe	Ti	Zr	Mn
20	1	8	43.2	25.6	9.5	15.1	3.5	0.0	3.1	0.0	0.0	0.0
20	1	9	58.4	1.9	0.0	20.9	18.8	0.0	0.0	0.0	0.0	0.0
20	1	10	41.5	31.1	8.3	14.5	1.7	0.0	2.8	0.0	0.0	0.0
20	1	11	56.0	27.0	6.9	7.8	0.0	0.0	2.3	0.0	0.0	0.0
20	1	12	46.2	15.1	5.8	14.3	7.0	4.8	6.7	0.0	0.0	0.0
20	1	13	31.6	36.4	5.8	24.1	0.0	0.0	2.0	0.0	0.0	0.0
20	1	14	53.8	8.3	0.0	22.2	15.7	0.0	0.0	0.0	0.0	0.0
20	1	15	41.6	27.9	9.8	14.8	2.3	0.0	3.6	0.0	0.0	0.0
20	1	16	40.9	34.7	8.1	13.5	0.0	0.0	2.8	0.0	0.0	0.0
20	1	17	56.0	0.0	0.0	21.9	11.8	10.2	0.0	0.0	0.0	0.0
20	1	18	41.6	33.2	7.9	14.2	0.0	0.0	3.1	0.0	0.0	0.0
20	1	19	44.9	30.2	6.4	14.6	1.4	0.0	2.6	0.0	0.0	0.0
20	1	20	44.7	27.3	7.5	15.0	2.4	0.0	3.2	0.0	0.0	0.0
20	2	1	53.2	4.0	0.0	22.1	1.7	19.1	0.0	0.0	0.0	0.0
20	2	2	42.8	12.9	8.7	15.6	5.2	9.6	5.2	0.0	0.0	0.0
20	2	3	46.9	15.2	6.2	14.2	7.1	4.6	5.9	0.0	0.0	0.0
20	2	4	2.1	70.6	14.1	6.8	0.0	6.5	0.0	0.0	0.0	0.0
20	2	5	38.8	24.1	3.8	15.0	5.2	0.0	13.0	0.0	0.0	0.0
20	2	6	33.6	21.7	11.3	16.6	0.0	0.0	16.9	0.0	0.0	0.0
20	2	7	43.2	11.9	9.0	15.8	5.3	10.1	4.8	0.0	0.0	0.0
20	2	8	46.0	16.4	7.0	14.4	6.1	5.0	5.3	0.0	0.0	0.0
20	2	9	46.8	16.1	6.6	14.1	6.2	5.0	5.3	0.0	0.0	0.0
20	2	10	50.8	19.0	7.4	14.2	6.0	0.0	2.6	0.0	0.0	0.0
20	2	11	46.6	23.5	9.3	14.5	3.6	0.0	2.6	0.0	0.0	0.0
20	2	12	46.0	15.8	6.2	14.1	7.0	4.8	6.1	0.0	0.0	0.0
20	2	13	46.7	22.5	8.7	15.7	3.9	0.0	2.5	0.0	0.0	0.0
20	2	14	45.1	24.9	9.1	15.3	2.9	0.0	2.8	0.0	0.0	0.0
21	1	1	48.9	21.9	8.7	17.4	3.2	0.0	0.0	0.0	0.0	0.0
21	1	3	74.3	0.0	0.0	13.7	7.5	4.5	0.0	0.0	0.0	0.0
21	1	4	69.9	1.7	0.0	15.2	7.3	5.9	0.0	0.0	0.0	0.0
21	1	5	45.3	19.9	8.5	16.1	2.9	3.5	3.8	0.0	0.0	0.0
21	1	6	44.1	0.6	0.0	12.2	16.7	0.0	26.4	0.0	0.0	0.0
21	1	8	73.3	0.0	0.0	14.4	7.2	5.1	0.0	0.0	0.0	0.0
21	1	9	70.2	0.0	0.0	16.3	7.1	6.4	0.0	0.0	0.0	0.0
21	1	10	42.1	18.0	6.5	14.2	2.5	0.0	15.2	1.5	0.0	0.0
21	1	11	49.7	18.3	7.9	14.6	3.0	3.4	3.0	0.0	0.0	0.0
21	1	12	46.1	19.5	8.4	16.2	3.6	3.3	3.0	0.0	0.0	0.0
21	1	13	43.8	14.8	4.9	14.2	2.5	4.6	15.1	0.0	0.0	0.0
21	1	14	64.3	2.3	0.0	18.8	7.8	6.8	0.0	0.0	0.0	0.0
21	1	17	55.4	2.6	0.0	19.6	6.4	7.1	7.1	1.9	0.0	0.0
21	1	18	44.6	22.6	8.1	15.7	2.4	0.0	6.6	0.0	0.0	0.0
21	1	19	42.9	25.7	8.0	14.8	2.1	0.0	6.5	0.0	0.0	0.0
21	1	20	49.7	8.9	0.0	27.0	9.5	4.9	0.0	0.0	0.0	0.0
22	1	2	43.5	28.1	8.5	13.9	3.0	0.0	3.0	0.0	0.0	0.0
22	1	3	42.3	29.1	8.9	14.1	2.5	0.0	3.1	0.0	0.0	0.0
22	1	4	42.7	28.7	9.0	14.0	3.1	0.0	2.5	0.0	0.0	0.0
22	1	5	39.7	28.0	9.3	13.4	2.6	0.0	7.0	0.0	0.0	0.0
22	1	6	43.9	26.5	8.7	12.5	3.1	0.0	2.8	0.0	2.5	0.0
22	1	9	50.8	18.3	6.9	12.3	6.0	3.3	2.4	0.0	0.0	0.0
22	1	10	45.8	25.2	7.9	16.1	2.7	0.0	2.4	0.0	0.0	0.0
22	1	12	46.9	25.0	8.0	14.2	3.4	0.0	2.5	0.0	0.0	0.0
22	1	13	45.7	25.1	8.2	15.0	3.4	0.0	2.6	0.0	0.0	0.0
22	1	14	45.4	24.6	8.5	15.4	3.5	0.0	2.7	0.0	0.0	0.0
22	1	15	42.2	30.0	8.6	13.8	2.8	0.0	2.8	0.0	0.0	0.0
23	1	1	30.3	49.7	3.1	15.5	0.0	0.0	1.4	0.0	0.0	0.0

475

Sample #	Area #	Point #	Si	Ca	Mg	Al	K	Na	Fe	Ti	Zr	Mn
23	1	2	29.8	53.4	2.3	14.4	0.0	0.0	0.0	0.0	0.0	0.0
23	1	3	31.3	54.1	3.1	11.6	0.0	0.0	0.0	0.0	0.0	0.0
23	1	4	31.5	52.9	2.9	12.7	0.0	0.0	0.0	0.0	0.0	0.0
23	2	1	0.0	59.2	40.8	0.0	0.0	0.0	0.0	0.0	0.0	0.0
23	2	2	32.5	49.6	5.8	12.0	0.0	0.0	0.0	0.0	0.0	0.0
23	2	3	60.1	23.9	2.8	12.0	0.0	0.0	1.2	0.0	0.0	0.0
23	2	4	31.1	54.6	0.0	14.3	0.0	0.0	0.0	0.0	0.0	0.0
23	3	1	32.0	47.0	3.2	17.8	0.0	0.0	0.0	0.0	0.0	0.0
23	3	2	32.3	44.2	4.0	19.5	0.0	0.0	0.0	0.0	0.0	0.0
23	3	3	31.9	40.3	4.9	21.3	0.0	0.0	1.5	0.0	0.0	0.0
23	3	4	31.4	42.5	4.6	19.9	0.0	0.0	1.5	0.0	0.0	0.0
23	3	5	32.3	39.7	5.4	21.0	0.0	0.0	1.6	0.0	0.0	0.0
23	3	6	32.3	43.9	4.5	19.3	0.0	0.0	0.0	0.0	0.0	0.0
23	4	1	31.6	48.4	3.3	16.7	0.0	0.0	0.0	0.0	0.0	0.0
23	4	2	59.2	31.9	0.0	8.9	0.0	0.0	0.0	0.0	0.0	0.0
23	4	3	23.9	63.1	3.3	9.8	0.0	0.0	0.0	0.0	0.0	0.0
24	1	1	35.4	38.8	10.2	12.4	0.0	0.0	3.1	0.0	0.0	0.0
24	1	6	47.0	21.9	8.8	13.8	2.8	3.1	2.5	0.0	0.0	0.0
24	1	7	42.5	34.2	7.5	11.2	2.8	0.0	1.9	0.0	0.0	0.0
24	1	8	47.9	17.8	5.7	16.8	4.8	5.1	1.9	0.0	0.0	0.0
24	1	9	44.5	23.6	9.2	13.5	2.8	3.7	2.8	0.0	0.0	0.0
24	1	10	55.7	17.9	7.6	14.1	2.7	0.0	2.1	0.0	0.0	0.0
25	1	2	45.8	22.4	9.3	16.2	3.1	0.0	3.1	0.0	0.0	0.0
25	1	4	63.2	0.0	0.0	19.1	10.3	7.4	0.0	0.0	0.0	0.0
25	1	5	88.8	0.0	0.0	7.2	4.0	0.0	0.0	0.0	0.0	0.0
25	1	6	57.0	0.0	0.0	21.4	12.0	9.7	0.0	0.0	0.0	0.0
25	1	7	11.7	56.1	0.0	2.8	8.5	0.0	20.9	0.0	0.0	0.0
25	1	9	9.0	46.4	0.0	1.0	43.7	0.0	0.0	0.0	0.0	0.0
25	1	10	34.8	17.9	0.0	9.6	18.7	0.0	18.9	0.0	0.0	0.0
25	2	1	50.2	21.9	10.2	17.7	0.0	0.0	0.0	0.0	0.0	0.0
25	2	2	43.6	28.0	10.6	13.7	1.6	0.0	2.5	0.0	0.0	0.0
25	2	3	51.0	19.6	8.8	15.0	3.9	0.0	1.6	0.0	0.0	0.0
25	2	4	5.9	68.9	0.0	0.0	3.9	0.0	21.4	0.0	0.0	0.0
25	2	5	49.4	20.4	8.2	14.7	4.1	0.0	3.2	0.0	0.0	0.0
25	2	6	24.3	55.2	0.0	1.9	5.7	0.0	12.9	0.0	0.0	0.0
25	2	8	52.9	16.0	8.0	13.0	3.5	3.5	2.1	1.1	0.0	0.0
25	2	9	50.5	7.6	0.0	27.3	2.5	12.1	0.0	0.0	0.0	0.0
25	2	10	36.4	23.4	0.0	9.6	18.7	0.0	11.9	0.0	0.0	0.0
25	2	11	58.6	3.2	0.0	20.7	11.8	5.7	0.0	0.0	0.0	0.0
25	2	12	58.9	1.3	0.0	19.6	17.4	0.0	2.8	0.0	0.0	0.0
25	2	13	22.8	0.0	0.0	11.4	4.1	10.0	51.6	0.0	0.0	0.0
25	2	14	61.5	0.0	0.0	23.6	14.9	0.0	0.0	0.0	0.0	0.0
25	2	15	13.9	0.0	0.0	6.9	2.0	7.6	67.4	0.0	0.0	2.3
25	2	16	59.8	0.0	0.0	21.3	13.2	5.7	0.0	0.0	0.0	0.0
25	3	1	36.9	25.9	14.6	16.0	1.8	0.0	4.8	0.0	0.0	0.0
25	3	2	32.6	11.1	48.4	5.9	0.0	0.0	2.1	0.0	0.0	0.0
25	3	3	33.5	9.2	50.5	5.1	0.0	0.0	1.6	0.0	0.0	0.0
25	4	2	52.7	19.3	6.9	13.6	4.5	0.0	3.0	0.0	0.0	0.0
25	4	3	92.0	0.0	0.0	5.2	2.8	0.0	0.0	0.0	0.0	0.0
25	5	6	86.7	4.3	0.0	5.5	3.5	0.0	0.0	0.0	0.0	0.0
25	5	8	48.5	22.6	6.9	14.1	4.3	0.0	3.6	0.0	0.0	0.0
26	1	1	49.8	23.1	7.7	13.7	2.6	0.0	3.1	0.0	0.0	0.0
26	1	2	48.7	23.1	8.2	14.9	2.3	0.0	2.7	0.0	0.0	0.0
26	1	3	48.3	23.2	7.9	15.0	2.6	0.0	2.9	0.0	0.0	0.0
26	1	4	48.2	23.6	8.0	15.1	2.2	0.0	2.9	0.0	0.0	0.0

Sample #	Area #	Point #	Si	Ca	Mg	Al	K	Na	Fe	Ti	Zr	Mn
26	1	5	47.7	23.7	8.1	14.9	2.4	0.0	3.1	0.0	0.0	0.0
26	1	6	48.0	23.6	8.0	15.3	2.2	0.0	2.9	0.0	0.0	0.0
27	1	7	55.2	15.2	6.6	12.1	3.7	4.8	2.4	0.0	0.0	0.0
27	1	8	52.9	15.8	6.0	14.7	2.9	5.1	2.7	0.0	0.0	0.0
27	1	9	67.2	9.5	4.2	8.8	3.7	4.7	1.9	0.0	0.0	0.0
27	2	1	53.2	16.6	6.5	8.7	7.7	3.8	3.6	0.0	0.0	0.0
27	2	2	56.7	15.5	5.8	12.1	3.0	3.9	3.0	0.0	0.0	0.0
28	1	1	40.1	28.9	10.1	18.4	0.0	0.0	2.5	0.0	0.0	0.0
28	1	2	39.6	31.0	9.0	17.6	0.0	0.0	2.8	0.0	0.0	0.0
28	1	3	39.4	30.1	9.8	18.1	0.0	0.0	2.6	0.0	0.0	0.0
28	1	4	39.2	29.7	10.2	18.4	0.0	0.0	2.6	0.0	0.0	0.0
28	1	5	39.1	29.1	10.5	19.0	0.0	0.0	2.3	0.0	0.0	0.0
28	1	6	39.2	29.7	10.4	18.2	0.0	0.0	2.6	0.0	0.0	0.0
28	1	7	39.0	30.1	10.0	18.5	0.0	0.0	2.4	0.0	0.0	0.0
28	1	8	38.9	30.2	9.9	18.4	0.0	0.0	2.6	0.0	0.0	0.0
28	1	9	38.8	29.9	10.2	18.4	0.0	0.0	2.6	0.0	0.0	0.0
28	1	10	39.3	30.0	9.7	18.4	0.0	0.0	2.6	0.0	0.0	0.0
29	1	1	58.4	0.0	0.0	21.1	14.5	5.9	0.0	0.0	0.0	0.0
29	1	2	45.9	24.5	9.6	13.8	3.8	0.0	2.4	0.0	0.0	0.0
29	1	3	13.4	21.6	51.9	9.5	0.0	0.0	3.5	0.0	0.0	0.0
29	1	6	4.4	88.9	2.8	3.9	0.0	0.0	0.0	0.0	0.0	0.0
29	1	7	64.1	3.9	0.0	17.2	8.7	4.6	1.4	0.0	0.0	0.0
29	1	8	40.8	30.1	9.4	14.0	2.2	0.0	3.5	0.0	0.0	0.0
29	2	1	39.7	13.2	4.7	8.2	3.0	0.0	0.0	0.0	31.3	0.0
29	2	5	49.6	21.2	7.8	15.4	2.7	0.0	3.3	0.0	0.0	0.0
29	3	1	58.4	0.0	0.0	21.4	14.3	6.0	0.0	0.0	0.0	0.0
29	3	2	40.9	29.5	9.7	15.2	1.7	0.0	3.1	0.0	0.0	0.0
29	3	5	63.9	3.5	3.3	16.6	10.6	0.0	2.0	0.0	0.0	0.0
29	3	8	46.9	23.9	7.8	15.6	3.2	0.0	2.5	0.0	0.0	0.0
29	3	9	43.0	27.8	8.5	14.8	2.8	0.0	3.3	0.0	0.0	0.0
29	3	10	43.0	27.8	8.5	14.8	2.8	0.0	3.3	0.0	0.0	0.0
29	3	11	34.6	41.8	9.0	9.5	1.8	0.0	3.3	0.0	0.0	0.0
29	3	12	40.1	31.4	9.6	14.3	1.8	0.0	2.9	0.0	0.0	0.0
29	3	13	47.3	23.1	8.1	15.5	2.2	0.0	3.8	0.0	0.0	0.0
30	1	2	57.2	0.0	0.0	20.9	7.8	14.1	0.0	0.0	0.0	0.0
30	1	3	46.2	22.4	8.9	16.0	2.9	0.0	3.6	0.0	0.0	0.0
30	1	5	58.8	0.0	0.0	21.1	16.2	4.0	0.0	0.0	0.0	0.0
30	1	6	58.0	0.0	0.0	24.9	10.1	7.0	0.0	0.0	0.0	0.0
30	1	8	49.1	8.1	0.0	28.4	4.6	9.8	0.0	0.0	0.0	0.0
30	1	9	46.9	21.2	9.7	16.2	3.3	0.0	2.7	0.0	0.0	0.0
30	1	11	61.8	0.0	0.0	20.5	13.5	4.3	0.0	0.0	0.0	0.0
30	1	12	60.4	0.0	0.0	21.5	14.0	4.0	0.0	0.0	0.0	0.0
30	1	14	46.8	10.8	0.0	30.7	4.0	7.7	0.0	0.0	0.0	0.0
30	1	15	43.7	24.5	9.9	16.6	2.2	0.0	3.1	0.0	0.0	0.0
30	2	2	49.2	22.1	10.6	18.1	0.0	0.0	0.0	0.0	0.0	0.0
30	2	3	43.7	32.0	4.1	11.9	2.6	0.0	5.7	0.0	0.0	0.0
30	2	4	47.8	19.2	9.9	17.1	2.9	0.0	3.1	0.0	0.0	0.0
30	3	1	48.9	20.2	8.7	15.5	3.8	0.0	2.9	0.0	0.0	0.0
30	3	2	43.9	0.0	0.0	36.6	11.5	4.4	3.5	0.0	0.0	0.0
30	4	2	49.1	2.3	0.0	8.8	4.4	0.0	0.0	0.0	35.4	0.0
31	1	1	59.3	0.0	0.0	21.5	14.8	4.5	0.0	0.0	0.0	0.0
31	1	2	54.2	4.7	0.0	24.7	9.5	6.9	0.0	0.0	0.0	0.0
31	1	4	69.5	0.0	0.0	15.3	9.9	5.4	0.0	0.0	0.0	0.0
31	1	5	36.5	31.1	8.8	22.1	0.0	0.0	1.5	0.0	0.0	0.0
31	1	6	45.5	26.6	8.5	13.3	3.3	0.0	2.8	0.0	0.0	0.0

Sample #	Area #	Point #	Si	Ca	Mg	Al	K	Na	Fe	Ti	Zr	Mn
31	1	7	44.8	26.7	8.4	14.8	2.6	0.0	2.6	0.0	0.0	0.0
31	1	8	51.3	4.3	0.0	25.1	13.4	5.9	0.0	0.0	0.0	0.0
31	1	11	77.0	0.0	0.0	16.5	6.6	0.0	0.0	0.0	0.0	0.0
31	1	12	59.6	0.0	0.0	21.4	19.0	0.0	0.0	0.0	0.0	0.0
32	1	1	49.4	26.7	8.2	13.4	0.0	0.0	2.2	0.0	0.0	0.0
32	1	2	48.8	25.8	8.7	14.3	0.0	0.0	2.3	0.0	0.0	0.0
32	1	3	48.4	29.9	6.1	12.8	0.0	0.0	2.8	0.0	0.0	0.0
32	1	4	49.7	27.0	7.7	13.1	0.0	0.0	2.6	0.0	0.0	0.0
32	1	5	49.3	26.3	8.4	13.5	0.0	0.0	2.4	0.0	0.0	0.0
32	1	6	49.5	25.7	8.8	13.7	0.0	0.0	2.3	0.0	0.0	0.0
32	1	7	49.1	26.8	8.2	13.5	0.0	0.0	2.4	0.0	0.0	0.0
32	1	8	49.3	27.3	7.9	13.2	0.0	0.0	2.2	0.0	0.0	0.0
32	1	9	49.3	27.2	8.0	13.5	0.0	0.0	2.0	0.0	0.0	0.0
32	1	10	48.9	26.9	8.1	13.7	0.0	0.0	2.4	0.0	0.0	0.0
32	1	11	49.1	26.9	8.2	13.8	0.0	0.0	2.0	0.0	0.0	0.0
32	1	12	49.1	27.1	8.1	13.4	0.0	0.0	2.2	0.0	0.0	0.0
32	1	13	49.0	27.1	8.2	13.5	0.0	0.0	2.2	0.0	0.0	0.0
33	1	1	66.3	3.1	0.0	16.4	9.2	5.0	0.0	0.0	0.0	0.0
33	1	2	56.6	4.0	3.6	19.1	7.6	7.0	2.0	0.0	0.0	0.0
33	1	3	44.6	21.2	11.6	14.4	1.9	3.9	2.4	0.0	0.0	0.0
33	1	7	59.0	0.0	0.0	20.8	14.5	5.6	0.0	0.0	0.0	0.0
33	1	8	58.5	0.0	0.0	21.8	11.3	8.4	0.0	0.0	0.0	0.0
33	1	9	67.1	0.0	0.0	17.2	12.0	3.7	0.0	0.0	0.0	0.0
33	1	11	79.6	0.0	0.0	12.7	7.6	0.0	0.0	0.0	0.0	0.0
33	1	13	44.7	23.2	8.6	16.7	3.3	0.0	3.5	0.0	0.0	0.0
33	1	14	45.3	21.8	11.9	14.9	2.4	0.0	3.7	0.0	0.0	0.0
34	1	1	44.2	21.4	8.7	15.5	3.2	3.6	3.4	0.0	0.0	0.0
34	1	2	44.7	25.0	7.8	13.7	4.2	0.0	4.6	0.0	0.0	0.0
34	1	3	47.1	24.0	8.3	15.5	2.5	0.0	2.7	0.0	0.0	0.0
34	1	4	48.1	24.2	9.0	16.0	0.0	0.0	2.6	0.0	0.0	0.0
34	1	5	50.7	19.6	7.7	16.4	2.7	0.0	2.9	0.0	0.0	0.0
34	1	6	47.0	24.1	6.4	17.0	2.9	0.0	2.6	0.0	0.0	0.0
34	1	7	49.1	20.6	7.9	16.4	2.6	0.0	3.3	0.0	0.0	0.0
34	1	8	59.2	6.8	0.0	20.6	9.8	3.6	0.0	0.0	0.0	0.0
34	1	9	96.3	0.0	0.0	2.2	1.5	0.0	0.0	0.0	0.0	0.0
34	1	10	98.7	0.0	0.0	0.0	1.3	0.0	0.0	0.0	0.0	0.0
34	1	11	47.7	23.3	8.4	15.1	2.4	0.0	3.1	0.0	0.0	0.0
34	1	12	47.5	23.4	8.4	15.5	2.4	0.0	2.9	0.0	0.0	0.0
34	1	13	46.4	23.7	8.4	15.6	2.9	0.0	3.1	0.0	0.0	0.0
34	1	14	44.7	25.5	9.4	14.4	3.1	0.0	3.1	0.0	0.0	0.0
35	1	1	57.8	8.3	3.5	15.5	8.8	3.7	2.4	0.0	0.0	0.0
35	1	2	45.6	22.3	7.7	14.7	3.8	3.4	2.5	0.0	0.0	0.0
35	1	3	45.8	22.8	8.0	15.0	2.8	3.5	2.1	0.0	0.0	0.0
35	1	4	43.7	26.4	9.5	16.9	1.6	0.0	2.0	0.0	0.0	0.0
35	1	5	44.0	26.3	9.1	15.9	1.8	0.0	2.9	0.0	0.0	0.0
35	1	6	45.2	30.8	4.1	11.8	4.4	0.0	3.6	0.0	0.0	0.0
35	1	7	47.2	24.3	7.9	15.0	2.6	0.0	2.9	0.0	0.0	0.0
35	1	8	47.7	24.6	7.7	14.9	2.2	0.0	2.9	0.0	0.0	0.0
35	1	9	49.9	23.1	8.2	13.5	2.4	0.0	2.9	0.0	0.0	0.0
35	1	10	46.2	25.3	8.1	15.5	2.2	0.0	2.8	0.0	0.0	0.0
36	1	1	52.2	22.1	7.6	13.8	1.8	0.0	2.5	0.0	0.0	0.0
36	1	2	50.3	22.8	8.4	13.3	2.3	0.0	2.9	0.0	0.0	0.0
36	2	1	50.8	24.2	7.9	14.3	0.0	0.0	2.9	0.0	0.0	0.0
36	2	2	49.6	24.7	8.2	14.8	0.0	0.0	2.8	0.0	0.0	0.0
36	2	3	50.8	23.1	7.9	13.4	2.0	0.0	2.9	0.0	0.0	0.0

Sample #	Area #	Point #	Si	Ca	Mg	Al	K	Na	Fe	Ti	Zr	Mn
36	2	4	48.4	26.4	7.1	15.6	0.0	0.0	2.4	0.0	0.0	0.0
36	2	5	49.8	24.7	8.1	15.0	0.0	0.0	2.5	0.0	0.0	0.0
36	2	6	48.4	24.7	8.0	13.2	2.4	0.0	3.3	0.0	0.0	0.0
36	2	7	48.8	25.7	8.1	14.7	0.0	0.0	2.6	0.0	0.0	0.0
36	2	8	49.3	25.6	7.9	14.5	0.0	0.0	2.6	0.0	0.0	0.0
36	2	9	94.0	0.0	0.0	4.0	2.0	0.0	0.0	0.0	0.0	0.0
36	3	1	49.7	17.1	7.4	11.8	7.0	4.0	3.0	0.0	0.0	0.0
36	3	2	43.3	34.1	6.7	13.2	0.0	0.0	2.8	0.0	0.0	0.0
36	3	3	43.8	32.6	7.6	13.5	0.0	0.0	2.5	0.0	0.0	0.0
37	1	2	47.3	23.5	8.3	14.8	2.8	0.0	3.3	0.0	0.0	0.0
37	1	5	46.3	24.2	8.4	15.8	2.2	0.0	3.0	0.0	0.0	0.0
37	1	6	95.5	0.0	0.0	3.2	1.3	0.0	0.0	0.0	0.0	0.0
37	1	7	46.4	23.3	8.4	15.6	3.3	0.0	2.9	0.0	0.0	0.0
37	1	8	74.5	0.0	0.0	15.2	10.3	0.0	0.0	0.0	0.0	0.0
37	1	10	46.3	23.9	9.0	16.2	1.8	0.0	2.9	0.0	0.0	0.0
38	1	2	60.8	0.0	0.0	21.9	17.3	0.0	0.0	0.0	0.0	0.0
38	1	3	46.5	23.9	9.2	14.9	2.6	0.0	2.9	0.0	0.0	0.0
38	1	5	46.7	22.8	8.3	15.6	3.3	0.0	3.3	0.0	0.0	0.0
38	1	8	45.8	25.5	7.8	15.5	2.6	0.0	2.8	0.0	0.0	0.0
38	1	9	8.2	83.7	2.3	3.6	0.0	0.0	2.3	0.0	0.0	0.0
38	1	10	69.7	0.0	0.0	17.6	12.6	0.0	0.0	0.0	0.0	0.0
39	1	1	47.4	24.3	8.3	15.1	1.9	0.0	3.0	0.0	0.0	0.0
39	1	2	47.8	24.0	8.2	15.2	1.9	0.0	2.8	0.0	0.0	0.0
39	1	3	47.5	23.8	8.4	14.8	2.4	0.0	3.1	0.0	0.0	0.0
39	1	4	48.3	23.8	8.2	14.7	2.2	0.0	2.7	0.0	0.0	0.0
39	1	5	68.8	0.0	0.0	14.4	9.4	5.0	2.3	0.0	0.0	0.0
39	1	6	47.8	24.1	8.3	15.1	2.0	0.0	2.6	0.0	0.0	0.0
39	1	7	41.3	32.3	9.9	12.0	1.5	0.0	3.0	0.0	0.0	0.0
39	2	1	34.9	34.3	18.4	12.3	0.0	0.0	0.0	0.0	0.0	0.0
40	1	1	50.2	31.6	0.0	18.2	0.0	0.0	0.0	0.0	0.0	0.0
40	1	2	52.2	12.2	3.1	21.9	6.6	4.0	0.0	0.0	0.0	0.0
40	1	6	5.5	75.8	5.2	11.0	0.0	0.0	2.6	0.0	0.0	0.0
40	1	7	49.1	22.1	7.7	14.4	3.5	0.0	3.1	0.0	0.0	0.0
40	1	8	47.1	23.5	8.2	14.7	3.5	0.0	3.0	0.0	0.0	0.0
40	1	9	7.1	59.2	5.8	22.3	0.0	0.0	5.6	0.0	0.0	0.0
40	1	10	44.5	26.9	8.3	14.4	2.6	0.0	3.3	0.0	0.0	0.0
41	1	1	0.0	53.6	46.4	0.0	0.0	0.0	0.0	0.0	0.0	0.0
41	1	4	21.6	71.4	4.2	2.8	0.0	0.0	0.0	0.0	0.0	0.0
41	1	5	36.6	33.5	13.7	12.2	1.4	0.0	2.5	0.0	0.0	0.0
41	1	7	4.9	18.0	67.2	7.0	0.0	0.0	2.9	0.0	0.0	0.0
41	1	8	57.5	0.0	0.0	21.2	12.9	8.5	0.0	0.0	0.0	0.0
41	1	9	46.5	24.4	8.6	15.0	2.9	0.0	2.6	0.0	0.0	0.0
41	1	10	44.5	25.9	9.6	16.1	1.3	0.0	2.6	0.0	0.0	0.0
41	1	11	43.4	27.6	8.9	14.5	2.4	0.0	3.2	0.0	0.0	0.0
41	1	13	41.4	24.7	15.1	13.4	2.6	0.0	2.8	0.0	0.0	0.0
41	1	14	39.2	23.2	10.4	15.4	2.3	0.0	9.4	0.0	0.0	0.0
41	1	15	37.1	34.5	13.9	11.9	0.0	0.0	2.6	0.0	0.0	0.0
41	1	16	42.2	28.9	9.9	13.9	2.5	0.0	2.7	0.0	0.0	0.0
42	1	1	58.9	0.0	0.0	22.2	15.1	3.9	0.0	0.0	0.0	0.0
42	1	2	54.0	4.1	0.0	25.2	11.3	5.4	0.0	0.0	0.0	0.0
42	1	6	45.7	25.5	8.4	13.7	3.6	0.0	3.0	0.0	0.0	0.0
42	1	8	46.8	11.9	0.0	28.1	7.1	6.1	0.0	0.0	0.0	0.0
42	1	9	45.5	24.8	8.5	15.2	3.2	0.0	2.8	0.0	0.0	0.0
42	1	10	43.8	26.9	9.1	14.5	2.4	0.0	3.3	0.0	0.0	0.0
42	1	11	43.9	26.4	9.3	14.7	2.6	0.0	3.0	0.0	0.0	0.0

Sample #	Area #	Point #	Si	Ca	Mg	Al	K	Na	Fe	Ti	Zr	Mn
42	1	12	45.9	25.1	8.4	14.7	3.2	0.0	2.6	0.0	0.0	0.0
43	1	2	42.7	35.8	5.7	11.7	1.6	0.0	2.5	0.0	0.0	0.0
43	1	3	41.0	30.3	9.4	14.0	2.6	0.0	2.6	0.0	0.0	0.0
43	2	1	42.7	36.0	5.6	11.5	1.7	0.0	2.5	0.0	0.0	0.0
43	2	2	41.2	30.4	9.0	14.3	2.6	0.0	2.4	0.0	0.0	0.0
43	2	3	42.5	29.3	8.0	14.4	2.8	0.0	3.0	0.0	0.0	0.0
43	2	4	44.8	26.5	8.3	13.7	3.7	0.0	3.0	0.0	0.0	0.0
43	2	5	40.2	31.2	6.2	20.5	0.0	0.0	1.9	0.0	0.0	0.0
43	2	6	41.8	29.5	8.2	14.6	2.5	0.0	3.4	0.0	0.0	0.0
43	2	7	47.0	27.5	7.5	15.6	0.0	0.0	2.4	0.0	0.0	0.0
43	2	8	46.7	26.6	8.3	15.7	0.0	0.0	2.6	0.0	0.0	0.0
43	2	9	47.5	26.6	7.8	15.7	0.0	0.0	2.4	0.0	0.0	0.0
43	2	10	47.8	26.4	7.9	15.5	0.0	0.0	2.4	0.0	0.0	0.0
43	2	11	47.4	26.6	7.6	15.9	0.0	0.0	2.4	0.0	0.0	0.0
43	2	12	46.4	27.2	7.7	16.3	0.0	0.0	2.4	0.0	0.0	0.0
43	2	13	47.3	26.9	7.8	15.8	0.0	0.0	2.2	0.0	0.0	0.0
44	1	1	71.8	2.1	0.0	16.9	9.2	0.0	0.0	0.0	0.0	0.0
44	1	3	51.5	17.4	7.8	16.7	3.5	0.0	3.0	0.0	0.0	0.0
44	1	4	53.3	16.4	7.1	16.9	3.1	0.0	3.1	0.0	0.0	0.0
44	1	5	38.9	27.8	14.9	13.4	1.5	0.0	3.6	0.0	0.0	0.0
44	1	6	49.7	21.8	8.2	15.1	2.6	0.0	2.6	0.0	0.0	0.0
44	1	8	48.8	22.1	7.9	15.2	3.1	0.0	2.9	0.0	0.0	0.0
44	2	1	71.8	2.1	0.0	16.7	9.4	0.0	0.0	0.0	0.0	0.0
44	2	4	40.3	28.3	14.8	13.3	0.0	0.0	3.4	0.0	0.0	0.0
44	2	5	51.8	16.0	7.3	15.1	3.7	3.2	2.8	0.0	0.0	0.0
44	2	8	59.2	1.7	0.0	21.6	12.9	4.6	0.0	0.0	0.0	0.0
44	2	9	60.4	0.0	0.0	21.9	14.2	3.5	0.0	0.0	0.0	0.0
44	2	10	72.6	1.8	0.0	16.4	9.3	0.0	0.0	0.0	0.0	0.0
44	2	11	57.3	9.3	4.3	15.6	7.0	5.0	1.5	0.0	0.0	0.0
44	2	12	68.6	1.7	0.0	16.7	9.5	3.6	0.0	0.0	0.0	0.0
44	2	13	46.5	23.5	8.7	15.2	3.0	0.0	3.0	0.0	0.0	0.0
44	2	14	43.2	25.8	10.3	15.3	2.2	0.0	3.2	0.0	0.0	0.0
44	2	16	47.5	17.4	7.2	17.0	3.8	4.1	2.9	0.0	0.0	0.0
44	2	17	60.1	3.7	0.0	22.0	7.0	7.0	0.0	0.0	0.0	0.0
44	2	18	48.0	23.1	8.7	15.3	1.7	0.0	3.1	0.0	0.0	0.0
44	2	19	49.6	11.4	0.0	27.9	5.7	5.5	0.0	0.0	0.0	0.0
45	1	1	36.2	33.0	9.3	21.5	0.0	0.0	0.0	0.0	0.0	0.0
45	1	2	47.9	25.7	8.2	15.1	0.0	0.0	3.1	0.0	0.0	0.0
45	1	3	48.8	25.7	7.8	14.9	0.0	0.0	2.9	0.0	0.0	0.0
45	1	4	48.1	26.1	7.6	15.0	0.0	0.0	3.1	0.0	0.0	0.0
45	1	5	48.4	25.9	7.7	15.2	0.0	0.0	2.9	0.0	0.0	0.0
46	1	1	48.8	22.5	6.3	18.6	1.7	0.0	2.2	0.0	0.0	0.0
46	1	2	49.5	20.7	9.4	17.9	0.0	0.0	2.6	0.0	0.0	0.0
46	1	3	46.7	26.0	6.0	21.3	0.0	0.0	0.0	0.0	0.0	0.0
46	1	4	48.6	19.9	8.6	14.8	1.9	3.9	2.4	0.0	0.0	0.0
46	1	5	51.0	19.1	9.7	11.4	2.6	4.1	2.2	0.0	0.0	0.0
46	1	6	59.7	7.8	0.0	21.3	4.0	7.2	0.0	0.0	0.0	0.0
46	1	7	66.2	2.2	0.0	17.4	5.8	6.3	2.0	0.0	0.0	0.0
46	1	8	54.1	14.7	5.6	16.2	2.4	4.7	2.4	0.0	0.0	0.0
46	1	9	54.9	18.0	6.7	10.9	2.5	4.6	2.3	0.0	0.0	0.0
46	1	10	60.7	8.4	2.6	17.0	6.0	5.3	0.0	0.0	0.0	0.0
46	1	11	57.5	14.8	0.0	16.6	3.5	5.4	2.2	0.0	0.0	0.0
47	1	2	64.6	5.9	0.0	18.3	4.3	4.7	2.3	0.0	0.0	0.0
47	1	3	64.0	5.6	0.0	18.8	4.7	4.9	2.0	0.0	0.0	0.0
47	1	4	67.8	2.2	0.0	18.1	6.5	5.4	0.0	0.0	0.0	0.0

Sample #	Area #	Point #	Si	Ca	Mg	Al	K	Na	Fe	Ti	Zr	Mn
47	1	5	62.5	6.5	0.0	19.4	4.3	5.0	2.3	0.0	0.0	0.0
47	1	7	78.7	5.2	0.0	9.4	2.8	4.0	0.0	0.0	0.0	0.0
47	1	9	79.9	4.2	0.0	9.8	2.6	3.5	0.0	0.0	0.0	0.0
47	1	10	69.9	5.1	0.0	16.1	4.4	4.4	0.0	0.0	0.0	0.0
47	1	11	96.6	0.0	0.0	2.2	1.2	0.0	0.0	0.0	0.0	0.0
47	1	12	60.4	7.7	0.0	20.7	3.6	5.0	2.7	0.0	0.0	0.0
47	1	13	71.7	1.8	0.0	15.1	6.7	4.7	0.0	0.0	0.0	0.0
48	1	1	42.7	23.9	9.1	15.2	2.3	3.8	3.0	0.0	0.0	0.0
48	1	2	48.5	23.3	7.9	15.2	1.8	0.0	3.3	0.0	0.0	0.0
48	1	3	47.7	24.1	8.2	15.9	1.5	0.0	2.6	0.0	0.0	0.0
48	1	4	48.2	23.6	7.9	15.8	1.5	0.0	3.0	0.0	0.0	0.0
48	1	5	48.6	24.4	8.1	16.1	0.0	0.0	2.8	0.0	0.0	0.0
49	1	1	44.1	28.1	6.6	18.6	0.0	0.0	2.6	0.0	0.0	0.0
49	1	2	45.4	27.7	7.1	17.2	0.0	0.0	2.6	0.0	0.0	0.0
49	1	4	57.4	21.0	6.1	10.6	0.0	0.0	5.0	0.0	0.0	0.0
49	1	5	47.0	25.6	8.5	15.3	0.0	0.0	3.5	0.0	0.0	0.0
49	2	1	43.4	28.4	7.1	18.4	0.0	0.0	2.8	0.0	0.0	0.0
49	2	2	44.8	28.5	7.3	16.7	0.0	0.0	2.6	0.0	0.0	0.0
49	2	3	59.1	21.4	6.1	11.3	0.0	0.0	2.0	0.0	0.0	0.0
49	2	5	43.1	27.5	9.1	14.9	1.7	0.0	3.7	0.0	0.0	0.0
49	2	6	44.3	26.2	8.1	18.8	0.0	0.0	2.6	0.0	0.0	0.0
49	2	7	75.4	0.0	0.0	13.2	7.9	3.5	0.0	0.0	0.0	0.0
49	2	9	48.2	25.6	8.2	14.9	0.0	0.0	3.1	0.0	0.0	0.0
49	2	10	45.6	26.1	10.3	14.7	0.0	0.0	3.2	0.0	0.0	0.0
49	2	12	49.8	25.2	6.9	15.1	0.0	0.0	3.0	0.0	0.0	0.0
49	2	13	59.0	21.7	5.9	11.1	0.0	0.0	2.3	0.0	0.0	0.0
50	1	1	57.1	2.4	0.0	23.2	7.1	10.3	0.0	0.0	0.0	0.0
50	1	3	59.8	0.0	0.0	21.1	19.1	0.0	0.0	0.0	0.0	0.0
50	1	4	59.2	0.0	0.0	21.5	19.3	0.0	0.0	0.0	0.0	0.0
50	1	5	40.8	26.3	8.0	13.4	2.4	0.0	9.1	0.0	0.0	0.0
50	1	6	40.5	26.8	9.4	13.9	1.9	0.0	7.5	0.0	0.0	0.0
50	1	7	41.5	25.7	8.2	13.8	2.4	0.0	8.4	0.0	0.0	0.0
50	1	8	44.8	25.3	8.5	15.9	2.4	0.0	3.1	0.0	0.0	0.0
50	1	9	44.2	26.8	7.9	15.8	2.9	0.0	2.4	0.0	0.0	0.0
50	1	10	48.3	22.7	5.5	14.8	5.2	0.0	3.5	0.0	0.0	0.0
50	1	11	47.7	18.0	7.5	15.7	5.1	3.5	2.6	0.0	0.0	0.0
50	1	12	23.9	17.3	9.8	9.4	0.0	0.0	35.8	4.0	0.0	0.0
50	1	13	33.8	41.7	7.8	13.6	0.0	0.0	3.1	0.0	0.0	0.0
50	1	14	45.9	24.3	8.7	15.7	2.8	0.0	2.6	0.0	0.0	0.0
50	1	15	31.7	26.3	11.6	12.3	2.2	0.0	3.7	12.3	0.0	0.0
50	1	16	2.9	14.3	74.5	4.0	0.0	0.0	2.3	2.0	0.0	0.0
50	2	1	27.1	30.6	25.1	10.4	0.0	0.0	3.1	3.7	0.0	0.0
50	2	2	44.8	27.1	5.9	14.0	3.6	0.0	3.6	1.0	0.0	0.0
50	2	3	29.2	27.3	12.7	10.5	1.7	0.0	2.6	15.9	0.0	0.0
50	2	4	36.6	28.4	12.8	13.3	1.9	0.0	2.9	4.1	0.0	0.0
50	3	1	0.0	0.0	9.6	0.0	0.0	0.0	90.4	0.0	0.0	0.0
50	3	2	6.3	34.5	38.7	9.5	0.0	0.0	7.3	3.7	0.0	0.0
50	4	1	25.5	14.7	10.9	11.5	0.0	0.0	35.4	2.0	0.0	0.0
50	4	2	27.7	14.5	11.9	12.5	0.0	0.0	33.3	0.0	0.0	0.0
50	4	3	25.3	14.0	11.6	12.2	0.0	0.0	36.9	0.0	0.0	0.0
50	4	4	26.4	15.7	10.9	12.1	1.4	0.0	31.4	2.0	0.0	0.0